Research Article

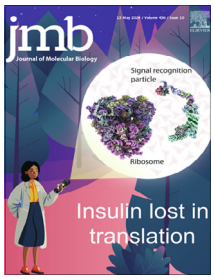

Transcriptomics Studies Reveal Functions of Transglutaminase 2 in Breast Cancer Cells Using Membrane Permeable and Impermeable Inhibitors

Pietro Ancona [1], Alessandro Trentini [2], Anna Terrazzan [1], Silvia Grassilli [2], Pauline Navals [3], Eric W. J. Gates [3], Valentina Rosta [2], Carlo Cervellati [1], Carlo M. Bergamini [4], Angela Pignatelli [4], Jeffrey W. Keillor [3], Cristian Taccioli [5] and Nicoletta Bianchi [1,*]

*1 - **Department of Translational Medicine,** University of Ferrara, 44121 Ferrara, Italy*
*2 - **Department of Environmental Sciences and Prevention,** University of Ferrara, Ferrara, Italy*
*3 - **Department of Chemistry and Biomolecular Sciences,** University of Ottawa, Ottawa, ON K1N 6N5, Canada*
*4 - **Department of Neuroscience and Rehabilitation,** University of Ferrara, 44121 Ferrara, Italy*
*5 - **Department of Animal Medicine,** Production and Health, University of Padua, Padua, Italy*

Correspondence to Nicoletta Bianchi:*Corresponding author. Address: Department of Translational Medicine, University of Ferrara, Via Luigi Borsari 46, 44121 Ferrara, Italy. *pietro.ancona@unife.it (P. Ancona), alessandro.trentini@unife.it (A. Trentini), anna.terrazzan@unife.it (A. Terrazzan), silvia.grassilli@unife.it (S. Grassilli), pnavals@uottawa.ca (P. Navals), egate028@uottawa.ca (E.W.J. Gates), valentina.rosta@unife.it (V. Rosta), carlo.cervellati@unife.it (C. Cervellati), bgc@unife.it (C.M. Bergamini), angela.pignatelli@unife.it (A. Pignatelli), jkeillor@uottawa.ca (J.W. Keillor), cristian.taccioli@unipd.it (C. Taccioli), nicoletta.bianchi@unife.it (N. Bianchi)*
https://doi.org/10.1016/j.jmb.2024.168569
Edited by Igor Stagljar

Abstract

Transglutaminase 2 (TG2) performs many functions both under physiological and pathological conditions. In cancer, its expression is associated with aggressiveness, propensity to epithelial-mesenchymal transition, and metastasis. Since TG2 performs key functions both outside and inside the cell, using inhibitors with different membrane permeability we analyzed the changes in the transcriptome induced in two triple-negative cell lines (MDA-MB-436 and MDA-MB-231) with aggressive features. By characterizing pathways and gene networks, we were able to define the effects of TG2 inhibitors (AA9, membrane-permeable, and NCEG2, impermeable) in relation to the roles of the enzyme in the intra- and extracellular space within the context of breast cancer. The deregulated genes revealed p53 and integrin signaling to be the common pathways with some genes showing opposite changes in expression. In MDA-MB-436, AA9 induced apoptosis, modulated cadherin, Wnt, gastrin and cholecystokinin receptors (CCKR) mediated signaling, with RHOB and GNG2 playing significant roles, and affected the Warburg effect by decreasing glycolytic enzymes. In MDA-MB-231 cells, AA9 strongly impacted HIF-mediated hypoxia, including AKT and mTOR pathway. These effects suggest an anti-tumor activity by blocking intracellular TG2 functions. Conversely, the use of NCEG2 stimulated the expression of ATP synthase and proteins involved in DNA replication, indicating a potential promotion of cell proliferation through inhibition of extracellular TG2. To effectively utilize these molecules as an anti-tumor strategy, an appropriate delivery system should be evaluated to target specific functions and avoid adverse effects. Additionally, considering combinations with other pathway modulators is crucial.

Introduction

Since the late 1990s, great attention has been paid to transglutaminase 2 (TG2) in breast cancer (BrCa), considering that TG2 is expressed at low levels in normal tissues, mainly in the extracellular matrix (ECM) around the ducts and in the endothelium, and it increases in intraductal cancers, assuming a borderline localization between tumor and normal tissues, with widespread distribution in the more invasive forms.[1,2] Indeed, the enzyme is present in both the extracellular and intracellular compartments, where it displays specific roles.

The expression of TG2 is regulated epigenetically depending on the degree of methylation of the *TGM2* gene that strongly correlates not only with aggressive features of BrCa cells[3] but also with response to drugs, such as inhibitors of histone deacetylase,[4] mTOR inhibitor rapamycin,[5] and tyrosine kinase,[6] making TG2 a potential target for the control of multidrug-resistance.[7] The induced changes under the control of TG2 chiefly concern cell modifications related to epithelial-to-mesenchymal transition (EMT),[8] leading to the loss of E-cadherin, a PARP3-mediated event in response to TGFβ-activation and reactive oxygen species (ROS) production sustained by the Snail1/Zeb1/Zeb2/Twist1 axis.[9]

The potential clinical relevance of TG2 as a risk factor for recurrence in patients with invasive ductal carcinomas,[10] soon became clear, identifying this protein as a marker of survival, stemness, drug-resistance and metastatic features.[11] One of the roles proposed for TG2 is the transamidation of keratin 19, which is highly expressed in BrCa, acting as a scaffold protein between TG2 and Src and increasing the kinase activity[12] upon overexpression of TG2 by EGF signaling cascade, involving Ras and Cdc42 pathways mediated by PI3K and NF-κB.[13,14] It is precisely the close relationship with NF-κB that sees TG2 as a protagonist in the inflammatory processes at the base of those changes,[15] displaying aggressive hallmarks of cancer within a positive TG2/NF-κB loop, maintaining high levels of TG2 and constitutively activated NF-κB,[16] aiding cell survival and invasiveness.[17] This pathway is mediated by intracellular TG2 activity, leading to I-κBα depletion due to its ubiquitin–proteasome degradation[18] or to phosphorylation forming the p52/RelB complex with overexpression of CD44.[19] TG2 displays both intracellular and extracellular roles improving EMT and metastatic dissemination.

Another extracellular function of TG2 can affect migration ability acting as a scaffold protein through interaction with S100A4 and syndecan-4,[20] as well as modulation of α5β1 integrin signaling to promote the deposition of fibrils in the ECM.[21] Thus, TG2 forms heteromeric complexes and interacts with other ECM proteins, such as collagens, stabilizing them. In particular, the secretion of TG2-enriched macrovesicles in the tumor microenvironment improved the migratory capacity of fibronectin-dependent metastatization.[22]

This multifunctional enzyme produces several tumorigenic actions in the extracellular space, not only through its transamidase catalytic activity and scaffold roles, but also through interactions with several extracellular domains of integrins, which trigger the focal adhesion kinase (FAK) cascade and an apoptosis-resistant phenotype.[23] Thus, it induces stress fiber assembly and actomyosin contraction, sustaining motility and migration of tumor cells. Furthermore, TG2 enhances these features through intracellular actions, such as interaction with vimentin to promote movement,[24] and fibronectin voltage-gated ion channels to affect membrane current.[25]

Intracellular functions of TG2 depend on its conformation, which is related to calcium and GTP concentrations. The role of TG2 as a G-protein has long been investigated in BrCa, proving to be pivotal for EMT.[26] Furthermore, the interaction with phospholipase Cδ1 seems to support the Akt/mTORC1 axis and autophagy in triple-negative BrCa cells (TNBC).[27] Inside the cells, TG2 can act like an enzyme to transamidate multiple targets, regulating cellular metabolism,[28,29] increasing the Warburg effect, activating of inflammation pathways through up-regulation of HIF-1α and MEK/ERK and LDH axis.[30]

For this reason, the inhibition of TG2 might be favorable from a therapeutic perspective in BrCa, because of its multifunctional roles impacting several cancer signatures (metabolism,[31] autophagy,[32] sensitivity to drugs,[33,34] EMT,[35] metastatization,[36] and apoptosis[37]). The interest in TG2 inhibitors is further improved by restoring PD-L1 inhibitor responsiveness to immunotherapy.[38]

Recently, Gates *et al.*[39] investigated the functions of TG2 by comparing the effects of membrane-impermeable *versus* (*vs*) permeable inhibitors, clarifying that the latter affect tumorigenic functions and suggesting a relevant intracellular role of TG2. However, we must consider that this two-sided enzyme in a biological complex context could play anti-cancer roles, deriving from the function displayed in the stroma[40] or depending on the relation with the GPR56 interplayer,[41] again by interactions with cellular matrix proteins, such as angiocidin.[42]

Therefore, this study aims to unveil the roles of TG2 in BrCa. With this purpose, we chose two cell lines, MDA-MB-436 and MDA-MB-231, widely employed in laboratories around the world as TNBC and circulating tumor cell models, which are of great interest to investigate BrCa metastatic potential, sustained by aggregation ability, adhesion, and migration.[43] As they only express TG2 among the transglutaminase members, we can in this manner exclude possible interference from other transglutaminases. We should underline that MDA-MB-436 cells exhibit higher basal levels

of both mRNA and TG2 protein than MDA-MB-231 cells[25] and show a different response to treatment, such as a greater sensitivity to AA9.[39] Both these cell types display negativity to estrogen receptor and positivity to vimentin, which correlate to invasive properties.[44] Despite the same phenotype and the high metastatic potential, these two cell lines show different degrees of invasiveness,[25] which is higher for MDA-MB-231, also presenting a greater proliferation rate and different cellular interconnection.[43] In addition, they exhibit different capabilities of remodeling of the extracellular matrix interacting with fibroblast synthesis of matrix metalloproteinases (MMPs).[45]

We investigated the deregulated genes and pathways by RNA-sequencing analysis and by using inhibitors with a specific cellular distribution. As a result, their effects could help further explain possible divergent functions of TG2.

Results

AA9, but not NCEG2, affects intracellular transamidase activity of TG2 in TNBC cells

To assess the effectiveness of the inhibitors AA9 and NCEG2 in inactivating the transamidase activity, we checked their effects on purified human recombinant TG2 *in vitro*. Both compounds presented similar efficacy, as reported by Gates *et al*.[39] However, NCEG2 and AA9 have different properties and activities related to their membrane permeability. NCEG2 remains in the extracellular space, unable to cross the plasma membrane, while AA9 is able to pass it easily.[39] This difference in permeability is crucial because it affects their ability to interact with the target, TG2. So, NCEG2 can primarily affect TG2 in the extracellular space (undetectable in our assay conditions), while AA9 can inactivate both extracellular and intracellular TG2. For these reasons, we analyzed their effects on the residual transamidase activity in cell lysates after treatment of the two TNBC cell lines, MDA-MB-436 and MDA-MB-231. Since in previous studies AA9 exhibited pro-apoptotic effects after 48 h of treatments at 50 μM[25,31] and displayed antiproliferative activity,[39] we used this concentration for further studies.

The basal transamidase activity in MDA-MB-436 is higher than in MDA-MB-231 cells, which displayed 46.07 ± 1.76%. After 1 h of exposure, only AA9 was able to inhibit the transamidase activity of TG2, with a residual percentage of 57.2 ± 5.2% (calculated comparing it to the control treated only with the vehicle), while NCEG2 cannot reduce it, showing 95.2 ± 8.4% residual activity in MDA-MB-436 cells. Similar results were obtained in MDA-MB-231 cells, in which AA9 inhibited the enzyme showing a residual activity of 34.5 ± 4.7%, while NCEG2 was fully ineffective with 102.8 ± 6.4% (values calculated with respect the own control cells, Figure 1A). The quantification of the TG2 protein by ELISA assay confirmed that this difference did not depend on the enzyme content (Figure 1B), which remained unchanged after 1 h exposure to the compounds.

AA9 and NCEG2 inhibit G-protein activities and affect conformation of TG2

TG2 is capable of large conformational dynamics, and it has been hypothesized that most irreversible covalent inhibitors of TG2 will lock the enzyme in its open conformation, preventing the formation of the GTP binding site and thus inhibiting its G-protein activity. In this context, we evaluated the effect of inhibitors AA9 and NCEG2 on the ability of TG2 ability to bind GTP. Briefly, the enzyme was incubated with each inhibitor at a concentration corresponding to two times their respective K_I value in a calcium-rich buffer that was later exchanged via dialysis to remove the calcium. BODIPY-GTP, a fluorescent GTP analogue, was then added to the solution at a constant concentration and the relative fluorescence values (RFU) were recorded. These values were compared to the signal of the BODIPY-GTP bound by uninhibited TG2, a positive control representing the maximum signal, as well as to a blank representing the intrinsic fluorescent signal of BODIPY-GTP in the absence of TG2. The results are presented in Figure 1C and show that both AA9 and NCEG2 prevent the fluorescent GTP analogue from binding to enzyme, resulting in fluorescent signals that are insignificantly different than that of the blank.

To correlate this inability to bind GTP to the conformational state of TG2, we analysed the enzyme by native polyacrylamide gel electrophoresis analysis (nPAGE), previously described as an effective method for differentiating between the two conformations of the enzyme. It has been clearly shown that the enzyme's open conformation migrates more slowly in nPAGE than its closed conformation.[46] Three controls were also analysed in this experiment: 1) uninhibited TG2 in the absence of GTP and in the presence of Ca^{2+}, serving as a positive control for the 'open' conformation, 2) uninhibited TG2 in the absence of both Ca^{2+} and GTP, corresponding to TG2 in its free forms and 3) uninhibited TG2 in the presence of GTP and in the absence of Ca^{2+}, corresponding to its 'closed' compact conformation. The effects of AA9 and NCEG2 were also evaluated by analysis by nPAGE, after preincubation of the enzyme at concentrations corresponding to twice their respective K_I values of the inhibitors. The results, shown in Figure 1C, clearly indicate that AA9 and NCEG2 lock TG2 exclusively in its open extended conformation that migrates as slowly as the calcium-rich control in which the open conformational state is formed.

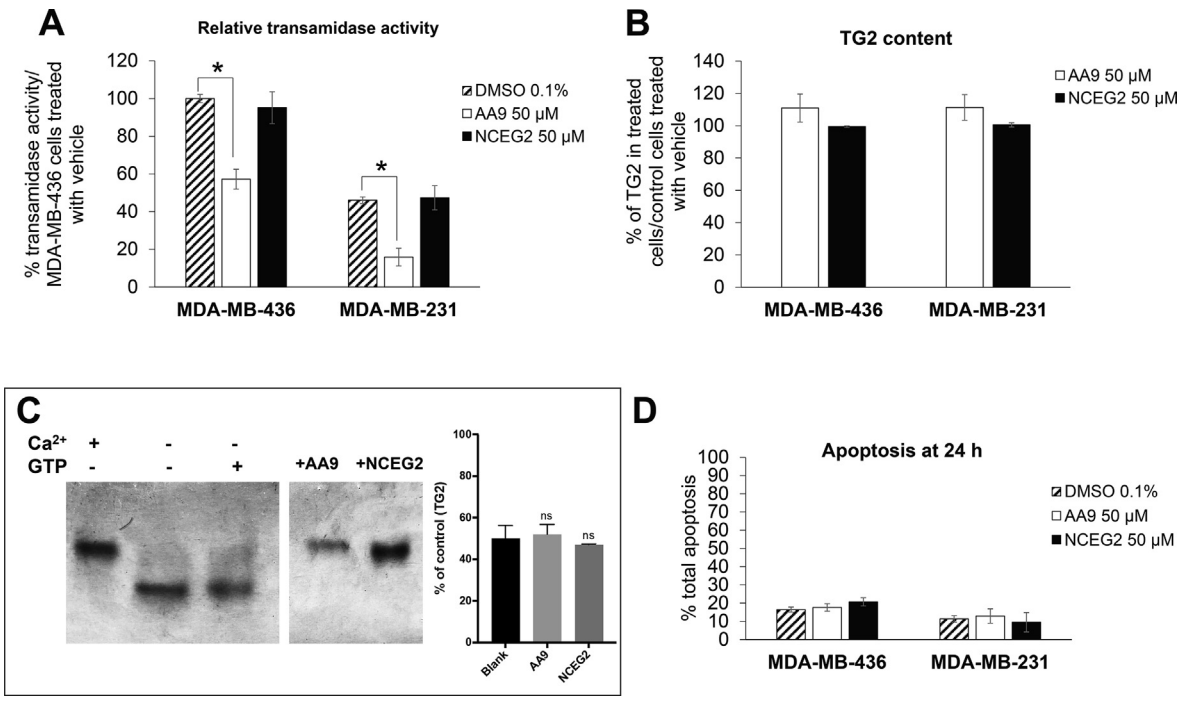

Figure 1. Effects of inhibitors in BrCa cells treated with TG2 inhibitors. (**A**) transamidase activity in cell lysates evaluated at 450 nm with an internal reference set at 540 nm (data were represented as percentage of MDA-MB36 cells treated with vehicle and assumed as control); (**B**) Amount of TG2 protein in the lysates quantified by ELISA assay (data were represented as percentage of respective samples treated with vehicle); (**C**) Evaluation of TG2 conformational dynamics and GTP binding ability after inhibition by inhibitors AA9 and NCEG2. On the left, GTP binding assay. Values are shown as percent of the maximum fluorescence observed for the positive control, in which TG2 was not inhibited prior to its binding to BODIPY-GTP. The blank represents the signal of the intrinsic fluorescence of the GTP analogue, in the absence of TG2 (ns = not significant; relative to the positive control of TG2 + BODIPY-GTP). On the right, conformational analysis of TG2 inhibited by inhibitors AA9 and NCEG2 by native PAGE. The gel shown here is contrast-adjusted; (**D**) Percentage of apoptosis after 24 h of treatment. Data were reported as average of three independent experiments ± SD. (*) *p*-value < 0.05 (Student's *t*-test, two-tail paired).

Transcriptome analysis highlights gene deregulation by TG2 inhibitors in BrCa cell lines

We hypothesized that a difference may exist in the intra- and extracellular functions of TG2 and we took advantage of the above inhibitors to define the specific changes occurring in the modulation of gene expression and the engaged pathways, after 24 h of treatment with 50 µM AA9 or NCEG2 on MDA-MB-436 and MDA-MB-231 cells by RNA-sequencing analysis and a bioinformatic approach. We focused on the early changes occurring before full-blown apoptosis complicated the picture of dysregulated genes, as verified in Figure 1D.

Principal component analysis (PCA) demonstrated similarities and differences between the groups of untreated and treated samples, while Supplementary Figure 1 reports their separated clustering. In the graphs, the inter- and intra-group variances were similar in the two analyzed conditions, despite some slight differences, with clear stratification of the samples that underwent treatment, suggesting that the use of these molecules influenced gene expression in both cell lines. In addition, the heatmaps generated for each cell line confirmed a stratification in agreement with that observed by PCA.

We found 5,125 significantly deregulated genes comparing MDA-MB-436 cells treated with AA9 *vs* DMSO, and 5,423 after treatment with NCEG2 *vs* DMSO (Supplementary files 1 and 2), while in MDA-MB-231 cells treated with AA9 *vs* DMSO, the dysregulated transcripts were 1,354 and 655 with NCEG2 *vs* DMSO respectively (Supplementary files 3 and 4). The representation of data through plotMA shown in Figure 2 well displays the difference between the paired groups, in which the significantly modulated genes are depicted in blue. These data are consistent with a greater impact of TG2 inhibitors on MDA-MB-436 than on MDA-MB-231 cells.

Genes and pathways deregulated by AA9 or NCEG2 in MDA-MB-436 cells

The Gene Set Enrichment Analysis (GSEA) demonstrated that only AA9 treatment significantly

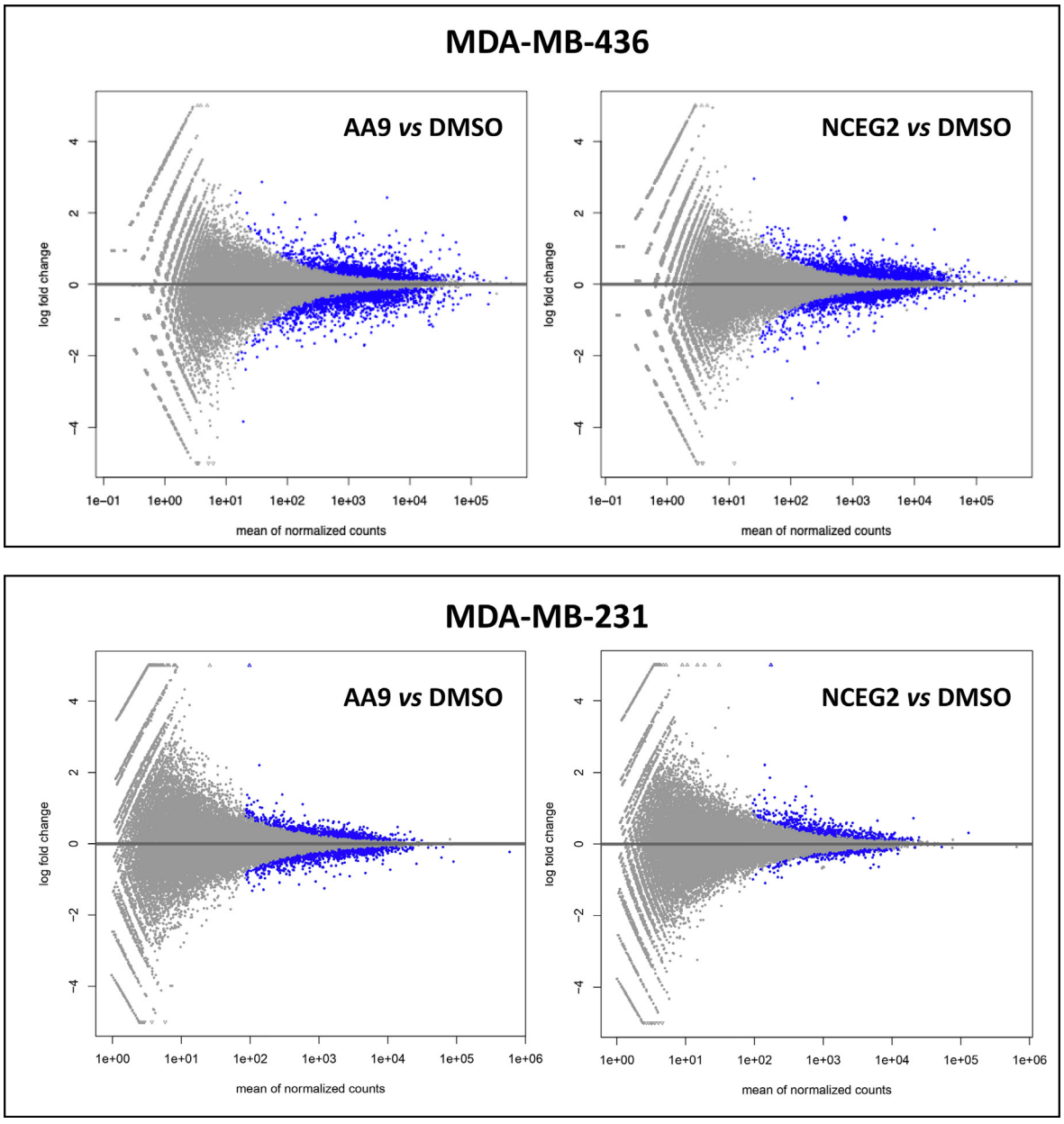

Figure 2. PlotMAs representation of gene expression following exposure of TNBC cells to TG2 inhibitors. The four graphs showed plotMAs, one of the graphical representations of the Bland-Altman method, used to analyse TNBC cell lines untreated or treated with TG2 inhibitors. At the top, MDA-MB-436, and bottom MDA-MB-231 cells. In the *y*-axis are reported, log2 FC values of each gene, while the *x*-axis describes the mean value of normalized counts of the transcripts. Genes are represented by spots: blue are those with a *p*-adj < 0.05, while grey spots correspond to insignificantly deregulated genes.

altered pathways (false discovery rate, FDR $\leq$ 0.05), as reported in Figure 3, four with negative enrichment values (P00012: cadherin signaling, P00004: presenilin related to Alzheimer's disease pathway, P00043: muscarinic acetylcholine receptor 2/4 signaling, and P00057: Wnt signaling), and one with a positive enrichment score (P06959: gastrin and cholecystokinin receptors (CCKR) mediated signaling). Treatment with NCEG2 did not reveal significant pathways with FDR $\leq$ 0.05, but one (P02740: *de novo* pyrimidine ribonucleotides biosynthesis) had a *p*-value < 0.05.

Over Representation Analysis (ORA) revealed significant transcriptional deregulation after both AA9 and NCEG2 treatment (Figure 4). We observed two commonly dysregulated pathways, the p53 (P00059) and the integrin signaling (P00034) pathways, while others appeared specific, as serine/glycine biosynthesis (P02776)

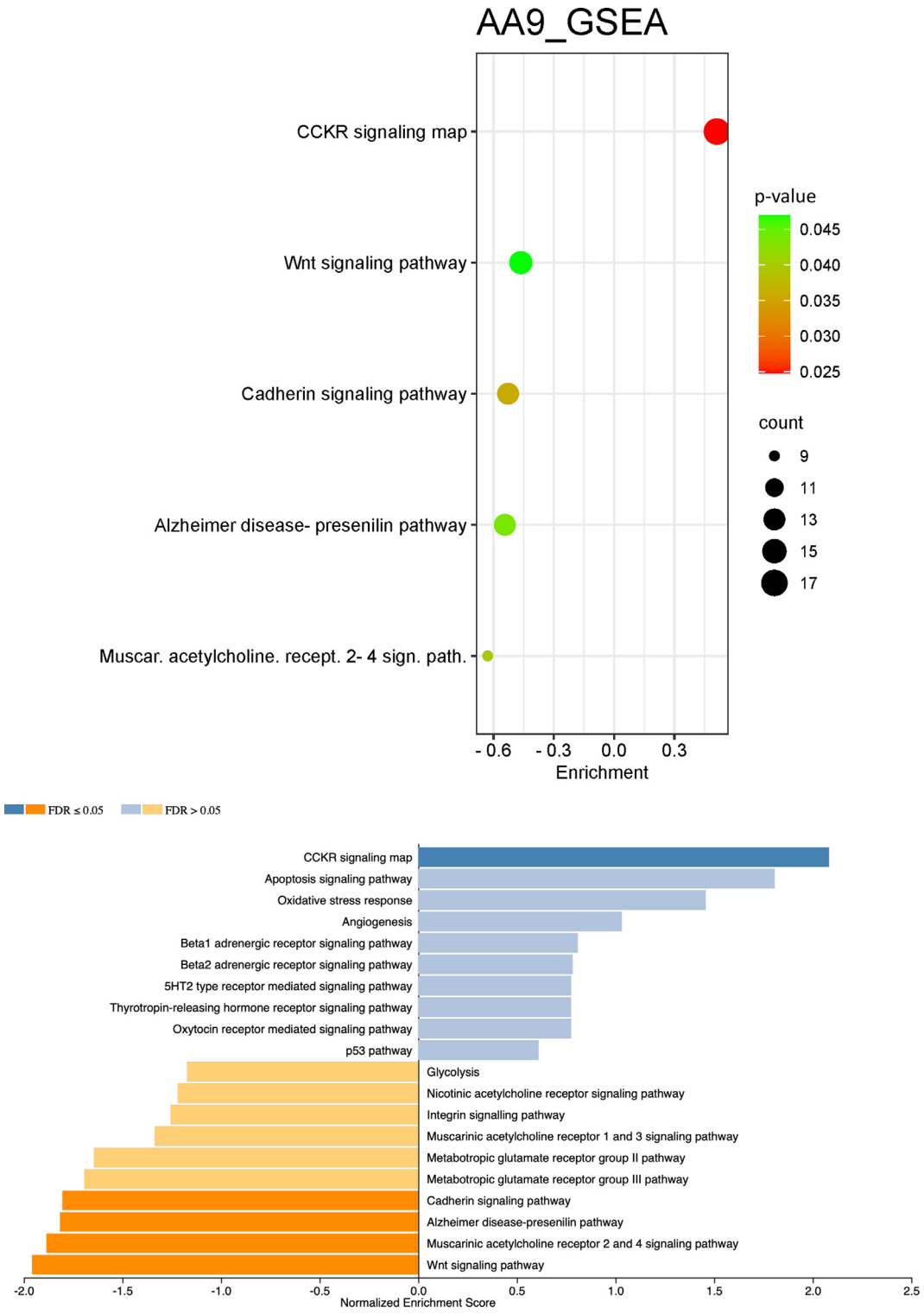

Figure 3. GSEA of MDA-MB-436 cells untreated and treated with AA9. Significantly altered expressed genes were used as an input list for the WebGestalt (adjusted *p*-value < 0.05). In **A**, the bubble plot is depicted, in which *x*-axis corresponds to pathway enrichment fold, while on *y*-axis the list of deregulated pathways is plotted. Each dot represents a specific pathway, where dot (or bubble) dimension corresponds to the number of genes of the input list found within the pathway. Color scale indicates the adjusted *p*-value associated to the enrichment of a specific pathway. In **B**, enriched pathways depicted as bar plot. The dark blue bars represent the significantly positive enriched, while the dark orange bars the significantly negative enriched pathways (FDR $\leq$ 0.05).

and *de novo* purine biosynthesis (P02738) pathways up-regulated and glycolysis (P00024) down-regulated by AA9, and DNA replication (P00017) and ATP synthesis (P02721) up-regulated by NCEG2.

Using Network Analyst we investigated the interconnections among the proteins encoded by the significantly deregulated genes in pathways from GSEA and ORA, as listed in Supplementary Figures 2 and 3. From the GSEA list, AA9 down-regulated genes in the cadherin and Wnt signaling pathways (WNT9A, WNT16, CTNNA2, PCDHGC3, and CELSR2), some of them interconnected with decreased matrix metalloproteinases (MMP1, MMP2, and MMP17) in the Alzheimer's disease presenilin pathway (Supplementary Figure 2); in addition, AA9 showed down-regulation of guanine nucleotide-binding proteins (GNB3, GNG4 and GNG7) and the SLCA8 transporter of creatine in the muscarinic acetylcholine receptor 2/4 signaling. In contrast, in the CCKR signaling we found up-regulation by AA9 of the axis GNG2/MYC/Serpine 1. For its relevance,[47] we checked the levels of GNG2 by Western blot demonstrating an increase of the coded protein in three independent experiments (Supplementary Figure 4A and B).

Concerning the unique networks emerging from ORA (Supplementary Figure 3A), AA9 increased phosphoglycerate dehydrogenase (PHGDH) in both biosynthetic pathways of serine/glycine and of *de novo* purine biosynthesis, interconnected with NME family genes, encoding nucleoside diphosphate kinases also markers of BrCa poor prognosis.[48] On the other side, NCEG2 increased energy supplying pathways, such as ATP synthesis, with up-regulation of several genes of ATP synthase F(1) complex (ATPF1A, ATPF1B, and ATPF1C), and POLA1 and other proteins involved in the DNA replication.

We uncovered some pathways common to both inhibitors, including deregulated genes belonging to the p53 pathway and integrin signaling. In the p53 pathway, the phosphoinositide-3-kinase regulatory subunit 3 decreased, whereas thrombospondin 1 increased after treatment with both molecules, while the other common genes displayed an opposite trend (Supplementary Figure 3B). Concerning the integrin signaling, both inhibitors affected the expression of many integrins, mostly down-regulated by AA9, some showing the same trend as NCEG2 (ITGA2, ITGA3, ITGA7, ITGB1, ITGB5, ITGAV), while others showing an inverse progression (ITGA5,

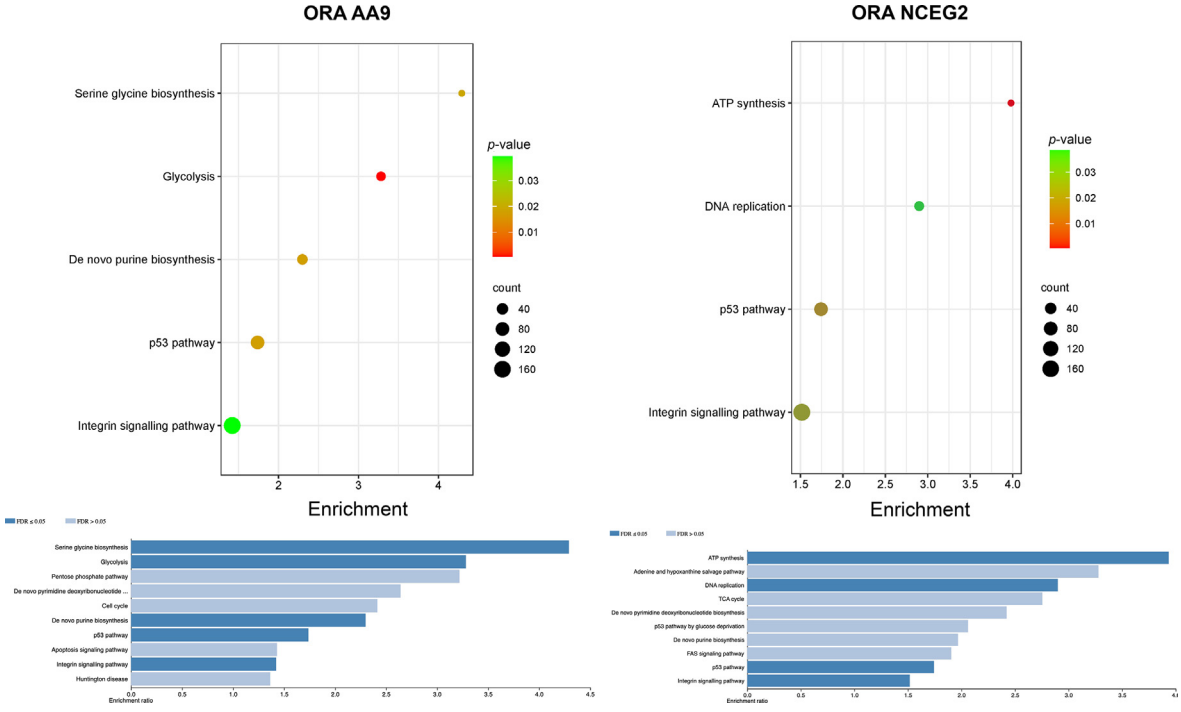

Figure 4. ORA of MDA-MB-436 cells untreated and treated with TG2 inhibitors. The list of the significantly altered expressed genes was used as input for the WebGestalt (adjusted *p*-value < 0.05). On the right, the comparison between AA9 *vs* DMSO, and on the left between NCEG2 *vs* DMSO. At the top, the bubble plot is depicted, in which *x*-axis corresponds to over-represented pathways, while in *y*-axis the list of deregulated pathways is plotted. Each dot represents a specific pathway, where dot (or bubble) dimension corresponds to the number of genes of the input list found within the pathway. Color scale indicates the adjusted *p*-value associated to enrichment of a specific pathway. At the bottom, dark blue bar plots depicted the over-represented and positive enriched pathways (FDR $\leq$ 0.05).

ITGA6, ITGA10). Among the common targets of the same pathway always with opposite trend, we found RHOB.

Finally, we focused on the top 100 deregulated genes (50 with positive and 50 with negative log2Fold Change, FC), emerging after treatment with AA9 or NCEG2 in MDA-MB-436 cells. We identified HKDC1, TAC1, GNG2, RHOB, ITGA10, CELSR2 cadherin, CHRM4, and MMP1 among the most deregulated by AA9 (Supplementary Figure 5, on the right) and COL13A1 among those altered by NCEG2 (Supplementary Figure 5, on the left), selected also based on their presence in functional GSEA and ORA analyses. We have validated the modulation of RHOB and MMP1 by reverse-transcription and quantitative polymerase chain reaction (RT-qPCR) (Supplementary Figure 4C). In addition, the amounts of MMP1 and COL13A1 proteins were measured by ELISA performed on cellular lysates and supernatants of the respective cultures, demonstrating a decrease of the secreted MMP1 after AA9 exposure for 48 h (intracellularly undetectable), whereas COL13A1 increased inside the cell with an external reduction (Supplementary Figure 4E). These data agreed with the down-modulation of several other genes coding enzymes and proteins involved in collagen modifications (PLOD2, P4HA1, PLOD1, LOXL1, PCOLCE).

Although not included in the list of transcripts reported as associated with the functional pathways, others were interesting because highly dysregulated after treatment with the inhibitors. Numerous were transporters of solutes and metabolites or regarded glucose metabolism: HKDC1, a newly identified kinase related to mitochondrial dysfunction, was one of the most up-regulated, whereas glycolytic enzymes were generally down-regulated, as 6-phosphofructo-2-ki nase/fructose-2,6-bisphosphatase, phosphofructokinase, enolase 1, glucose-6-phosphate isomerase and phosphoglycerate kinase 1. The largest group of genes dysregulated by AA9 (about 60 targets) concerned metabolism, as glycolysis and reduction of pyruvate (lactate dehydrogenase A), UDP-N-acetylglucosamine pyrophosphorylase 1, acyl-CoA synthetase short-chain family member 2, asparagine synthetase, uridine phosphorylase 1, thioredoxin reductase 1, malic enzyme 1 and other NADP(H) dehydrogenases, in addition to inositol-3-phosphate synthase 1, X domain containing 1 of phosphatidylinositol-specific phospholipase C and phospholipase Cβ4. Interestingly, also iron metabolism seemed to be altered, promoting the expression of both light and heavy chain 1 of ferritin (FTH1, they are claimed of anticancer properties[49] and heme oxygenase 1 (HMOX1) the latter one of the most up-regulated and relevant in cancer progression.

Among the 100 genes deregulated by NCEG2 (50 with positive and 50 with negative log2FC), beyond COL13A1 included in ORA, we noted increased expression of some cancer-related genes (Supplementary File 2): TGF-β-mediated keratin-associated protein 2–3 (KRTAP2-3) promoting migration by inducing EMT, and CDK15 cyclin regulating β-catenin via MEK-ERK signaling cascade and a marker of poor prognosis in BrCa, as well as acyl-CoA oxidase 2 (ACOX2) acting via PPARα pathway. On the other hand, the most deeply down-regulated genes were NUPR1, encoding a transcription factor with repressor function of ferroptosis and involved in the cell antioxidant power, and growth differentiation factor 15 (GDF15), a bone morphogenetic protein (BMP) and member of the TGF-β superfamily.

Genes and pathways deregulated by AA9 or NCEG2 in MDA-MB-231 cells

With the same experimental rationale, we analyzed the effects of AA9 and NCEG2 on the other TNBC cell line MDA-MB-231, performing GSEA on the dataset of genes deregulated by treatment with AA9 or NCEG2. We did not find statistically significant enriched pathways (considering FDR $\leq$ 0.05), despite two having *p*-value < 0.05, the cytoskeletal regulation by Rho GTPase (P00016) with up-regulation of tubulins by AA9, and the Toll receptor signaling pathway with induction of NF-κB inhibitor α (NFKBIA) and TNFα-induced protein 3 (TNFAIP3) by NCEG2. Instead, ORA allowed to identify three pathways enriched (FDR $\leq$ 0.05) upon treatment with AA9 (Figure 5), i.e. hypoxia response *via* HIF activation (P00030), p53 pathway feedback loops 2 (P04398) and p53 pathway (P00059), but no pathway significantly modified by NCEG2. Supplementary Figure 6 showed down-regulation of AKT2 and AKT3 in all the AA9-modulated networks. The expression of *AKT2* has been validated by RT-qPCR in independent experiments (Supplementary Figure 4D). The p53 pathway feedback loops 2 included MYC also down-regulated, but up-regulated by AA9 in the CCKR signaling of MDA-MB-436 cells.

MYC and cyclin-dependent kinase inhibitor 1A (CDKN1A) appeared important from a more extensive evaluation, focusing on the top 100 genes dysregulated by AA9 (Supplementary Figure 7). Among the most overexpressed transcripts, we found tumor necrosis factor receptor 9 (TNFRSF9), while among the most decreased were DEPTOR, a negative regulator of mTOR, Hyaluronan synthase 2 (HAS2), associated with progression, migration, metastatization, and Arrestin Domain Containing 4 (ARRDC4), binding GLUT1 to stimulate its endocytosis, inhibiting glucose uptake.

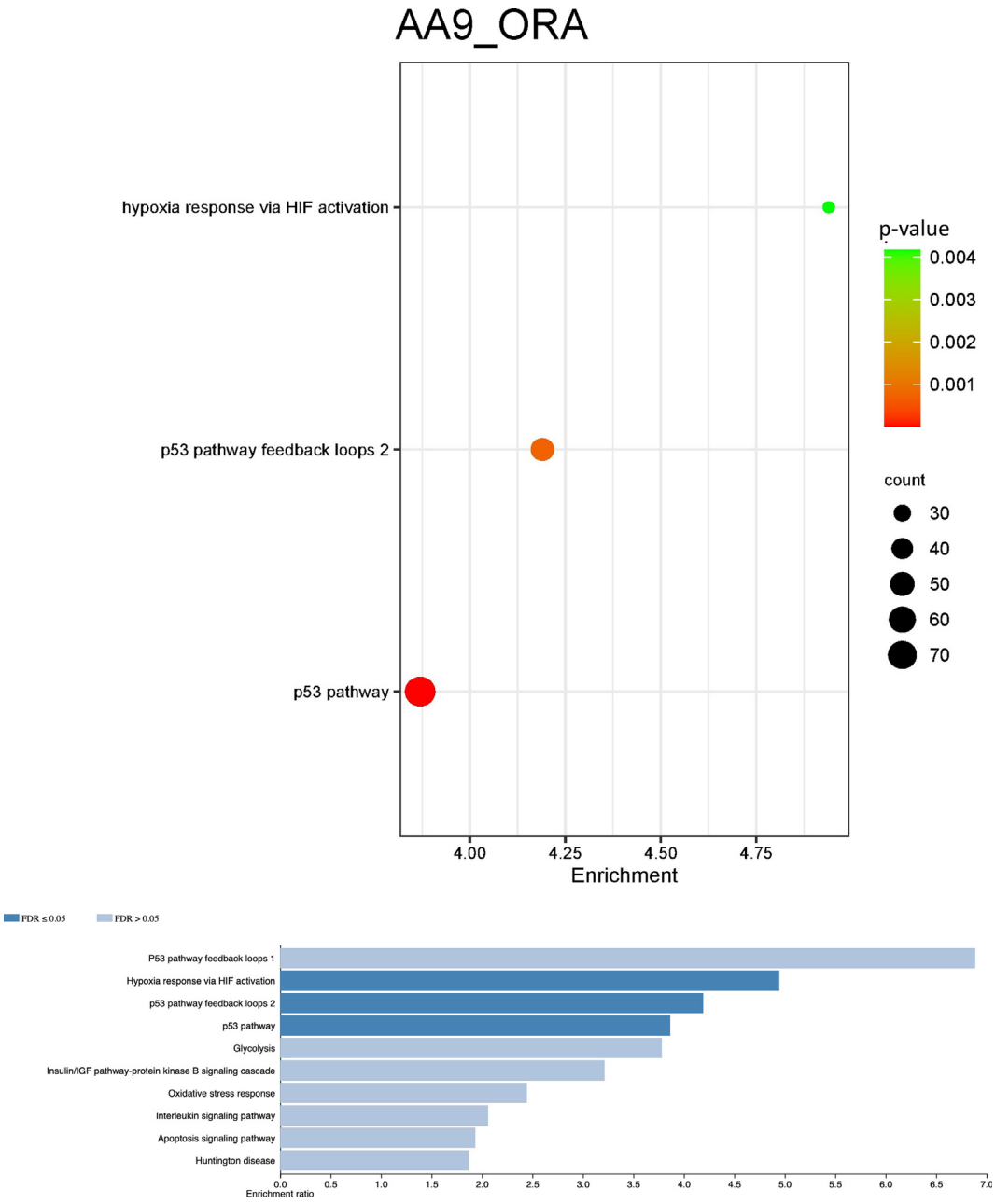

Figure 5. ORA of MDA-MB-231 cells untreated and treated with AA9. Significantly modulated genes were used as an input list for the WebGestalt (adjusted *p*-value < 0.05). In **A**, the bubble plot is depicted, in which the *x*-axis corresponds to over-represented pathways, while on *y*-axis the list of deregulated pathways is plotted. Each dot represents a specific pathway, where the dot (or bubble) dimension corresponds to the number of genes of the input list found within the pathway. Color scale indicates the adjusted *p*-value associated to enrichment of a specific pathway. In **B**, over-represented pathways, of which the significantly positive enriched are depicted as dark blue bar plot (FDR $\leq$ 0.05).

Regarding the effects mediated by NCEG2 on the top 100 dysregulated genes, we found again increased TNFRSF9 and decreased Rhomboid Like 1 (RHBDL1), a serine-type endopeptidase releasing polypeptides from the membrane as bioactive ligands, together with cell adhesion molecule 2 (CADM2) (Supplementary Figure 7).

Common genes associated with treatments or cell type

Comparing the AA9 treatment on MDA-MB-436 and MDA-MB-231 cells, we found 545 shared deregulated genes, while in the case of NCEG2 treatment the number was much lower, equal to 257 genes. Both AA9 and NCEG2 displayed

extracellular effects because AA9 remains outside the cell before entering. This reasoning explains how they could affect 39 total common targets.

To further narrow the field to the top 100 deregulated genes, we summarized them in the Venn diagram of Figure 6. After treatment with AA9 we noted a similar trend in both cell lines for HMOX1, sphingosine-1-phosphate phosphatase 2 (SGPP2) and the Ca^{2+}-activated Cl^{-} channel Bestrophin-1 (BEST1) that increased, while laminin subunit β 2 pseudogene 1 (LAMB2P1) decreased. Notably, both cell lines, NCEG2 promoted overexpression of two non-coding RNA (ncRNA) related to Ankyrin Repeat Domain 36.

Concerning the deregulated genes by both inhibitors, other ncRNAs were in MDA-MB-436 (ENSG0000275209; ENSG00000274224; ENSG00000278597; LINC00887) and in MDA-MB-231 (AC083837.1). In addition, in MDA-MB-436 cells both inhibitors affected KRTAP2-3, while the cyclin CCND2 and the interconvertible enzyme xanthine dehydrogenase (XDH) showed an inverse trend compared to MDA-MB-231 cells. Here, TNFRSF9, TNFAIP3, NFKBIA, and the scavenger receptor class A member 3 (SCARA3) were similarly modulated by both inhibitors, while HAS2 presented an inverse trend (Figure 6).

Discussion

The aim of the study was to assess the specific roles played by TG2 in the intracellular and extracellular compartments, using the inhibitors AA9 and NCEG2, which are permeable and impermeable to the cell membrane, displaying the advantage to inhibit the enzyme in specific cellular location. In opposite, the use of RNA interference (iRNA) or knockout techniques would inhibit or suppress the global production of the protein without distinguishing functional properties associated with its localization. Furthermore, gene knockout with an absolute absence of the protein would force cells to rearrange their transcriptional profile, activating compensatory mechanisms for survival. Under these conditions, the expression of other members of the TGase family could be reactivated driving different pathways in comparison with the functional enzymatic deficiency.[50,51] The use of the simple application of small molecules compared to treatments with iRNAs avoids complicate delivery systems and is helpful to understand the specific effects of TG2 inhibitors in the perspective of clinical trials, such as celiac disease.[52,53]

Our strategy was to evaluate changes in gene expression on the TNBC cells, MDA-MB-436 and MDA-MB-231, which have different content of TG2.[25] Accordingly, the evaluation of transamidase activity displayed lower basal values in MDA-MB-231 than in MDA-MB-436 cells, so that the inhibitory effect of AA9 is proportionally comparable in both lines and, as expected, only this inhibitor affected the intracellular transamidase activity. By performing an integrative analysis of the transcriptome obtained through RNA-sequencing, we identified specific and common pathways influenced by TG2. Considering the similarities and the differences in tumor features, we examined the effects of these potential anti-tumor inhibitors on cellular response by short-term treatment (24 h), before the occurrence of apoptosis (Figure 1D). We observed a significantly lower number of deregulated genes in MDA-MB-231 (1,354 by AA9 and 655 by NCEG2) compared to MDA-MB-436 cells (5,125 by AA9 and 5,423 by NCEG2), indicating a greater sensitivity of the latter to the TG2 inhibitors.

This transcriptomic approach must give answer to relevant questions on TG2 in the intracellular and extracellular compartments.

The first question is: “Are there common pathways druggable in these types of BrCas?”

Notably, this occurred in the cell response to AA9. Both cell lines present a *TP53* mutation, which in MDA-MB-436 produces a frameshift with stop of translation (p.R202Xfs, https://cancer.sanger.ac.uk/cosmic) and absence of protein,[54] while in MDA-MB-231 cells the mutation (p.Arg280Lys, c.839G > A) codes an overexpressed protein with altered unknown function.[55] These mutations define an aggressive phenotype of these BrCa cells, due to the alteration of this important tumor suppressor. In MDA-MB-231 (Supplementary Figure 6) and in MDA-MB-436 cells (Supplementary Figure 3), exposure to AA9 altered pathways highlighting an impact of a set of genes related to the p53 pathway. This led to induction of apoptosis in MDA-MB-231 cells, increasing transcripts coding CDKN1A and tumor-suppressor genes (PTEN, EP300, ZMAT3, and TNFRSF10B), especially decreasing the levels of AKT2 and AKT3, also included in the hypoxia pathway. In agreement with these data, the onco-suppressor and pro-apoptotic factor TNFRSF9 was increased by AA9 (Supplementary Figure 7) now emerging as a target to ameliorate immunotherapy controlling the p38MAPK/PAX6 signaling cascade,[56] and the strong decrease of Deptor inversely correlates with metastasis and chemoresistance.[57] This strengthens the hypothesis that the anti-oncogenic effect of AA9 is related to intracellular TG2. Furthermore, the down-regulation of MYC and the simultaneous up-regulation of the tumor-suppressor RB1 in the p53 pathway feedback loop 2 agreed with the anticancer effects of AA9. Analogously, in MDA-MB-436 cells this inhibitor affected several shared genes belonging to the p53 pathway, such as CDKN1A, TNFRSF10B, and AKT2. These findings agree with the previous observation that AA9 induced apoptosis on longer-time intervals,[39] and they suggest it could be considered for applications to these cancer phenotypes, perhaps in combination with other

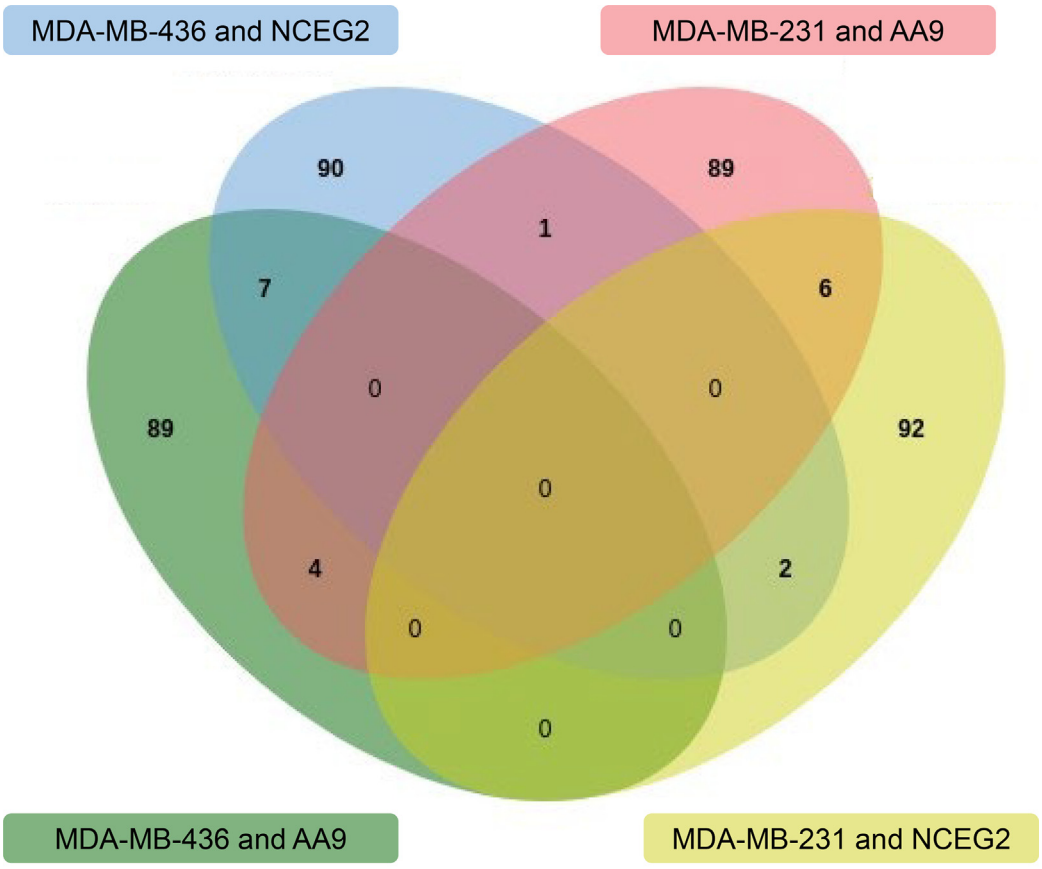

common to AA9 treatment in both cell lines	common to NCEG2 treatment in both cell lines	common to both inhibitors in MDA-MB-436	common to both inhibitors in MDA-MB-231
↑ HMOX1	↑ nc-ANKRD36-1:8 (ENSG00000277701)	↑ KRTAP2-3	↑ AC083837.1
↑ SGPP2	↑ lnc-ANKRD36B-3:17 (APPAT)	↑ FP236383 (ENSG0000275209)	↑ TNFRSF9
↑ BEST1		↑ ENSG00000274224	↑ NFKBIA
↓ LAMB2P1		CCND2*	↑ TNFAIP3
		↑ FP671120 (ENSG00000278597)	↑ SCARA3
		XDH**	HAS2**
		LINC00887**	

* ↑ AA9 and ↓ NCEG2; ** ↓ AA9 and ↑ NCEG2

Figure 6. Venn Diagram. This graph shows common overlapping deregulated genes after treatments with AA9 or NCEG2 in the two cell lines (MDA-MB-436 or MDA-MB-231).

drugs already employed to control proteins involved in these pathways.

The second question is: "Do the TG2 inhibitors impact the same pathways?"

Both inhibitors modulate some shared network of genes, but, essentially, they led to different effects. Indeed, concerning the p53 pathway in MDA-MB-436 cells, NCEG2 modulated some genes

mentioned above but showing an inverse trend (i.e. AKT2, Supplementary Figure 3). This implies that TG2 might have opposite roles inside and outside the cell.

Beyond the p53 pathway, we found integrin signaling among the commonly altered pathways (Supplementary Figure 3). As AA9 may also act on extracellular TG2 before penetrating the cell, it is plausible that some effects could be similar; so, several integrins (mainly down-regulated) showed comparable changes. For example, we observed decreased expression of ITGA2 and ITGB1 using both inhibitors, and this is reported to be associated with malignant phenotype and EMT promotion, due to a decreased binding between α2β1 Integrin and Laminin,[58] as it happens for the genes coding the subunits of α3β1,[59] and αvβ1 Integrins,[60] the *ITGA7* marker of low survival prognosis,[61] and *ITGB5* correlated to EMT.[62] Acting in the extracellular space, these inhibitors bind to the catalytic site of TG2, but they are not necessarily inert with respect to non-catalytic functions. Since they modify the conformation of TG2 from closed to opened in an irreversible manner (Figure 1C), so they may lead to repercussions on the non-catalytic activities of the protein, such as the interaction between fibronectin and integrin. In fact, TG2 binds integrin with its β-barrel 2 domain and fibronectin with its β-sandwich in the closed conformation; hence an open conformation could alter their distance or the conformational of the complex, triggering downstream effects. Indeed, we observed modified signaling pathways also after treatment with extracellular NCEG2, leading to modulation of integrin gene expression.

Another question concerns the integrins with inverse modulation. Interestingly, we observed a AA9-mediated decrease of the transcripts ITGA5 (associated with tumor progression *via* TWIST[63] and ITGA6 (associated with resistance to radiotherapy via Akt/Erk signaling,[64] and ITGA10, which were conversely overexpressed by NCEG2 (Supplementary File 3). These data illustrate the distinct effects related to inhibition of TG2 in different cellular locations.

It is known that in the extracellular space TG2 interacts with fibronectin and β1 integrin receptor[65] but also with integrin-linked kinase, modulating Wnt and β-catenin signaling.[66] In this respect, we identified different deregulated genes and pathways depending on the inhibitor used. We observed a decrease in cadherin and Wnt signaling (Figure 3) only after AA9 treatment, with low expression of WNT16 and WNT9A and the αN-catenin CTNNA2 (Supplementary Figure 2). Therefore, this might interfere with the localization of E-cadherin and actin polymerization,[67] suggesting an attempt to escape apoptosis.[68] This response could be counteracted by the AA9-mediated increase of RHOB, identified in the integrin signaling by ORA (Supplementary Figure 3) and reported in the Volcano plot (Supplementary Figure 5). The opposite regulation of RHOB in MDA-MB-436 cells (up by AA9 and down by NGEG2), such as some above reported integrins, could correlate with less aggressive features. RHO/ROCK-signaling controls the dynamics of the cytoskeleton.[69] As vimentin is a preferred well-known substrate of RHO,[70] we attribute what we observed to the changes in the interactions between intracellular TG2 and vimentin, which is modified following treatment with other permeable inhibitors, such as NC9, causing a shift of TG2 location to perinuclear/nuclear area.[24] Also, RHOB could be a central player in these networks. Furthermore, the structures of cytoskeleton are also involved in secretion of MMPs, to which TG2 notoriously participates.[71] A crucial downstream effect of AA9 in MDA-MB-436 cells, is the lower levels of MMP1 transcript (Supplementary Figure 2). This is a marker associated with poor prognosis[72] and its reduction limits invasiveness.[73] Accordingly, we found lower levels of other MMPs (MMP2,[74] MMP14,[75] and MMP17[76]) likewise associated with invasion and metastasis. Notably, the level of MMP1 protein decreased in the supernatant of the AA9-treated cells (validated in Supplementary Figure 4). In this case NCEG2 displayed opposite effects, increasing MMP1 in the supernatant and instead impacting another secreted protein, the collagen COL13A1 (Supplementary Figure 5 and validated in Supplementary Figure 4), which was overexpressed and accumulated inside the cells after the administration, with a decrease in the extracellular amount. The relationship of TG2 with MMP1 and collagen has been demonstrated to affect cancer growth in a TG2-knockout mouse model.[77] Several other genes coding enzymes involved in collagen modifications were also modified.

The third question is: “Can AA9 and NCEG2 unveil unique functions, in order to attribute them to an exact extracellular or intracellular compartment?”

Specific pathways emerged by GSEA analysis in MDA-MB-436 cells (with robust value of significance, FDR $\leq$ 0.05) following the intracellular inhibition of TG2 by AA9. Among the up-regulated pathways, we found CCKR signaling (Figure 3), working in balance with the Rho GTPase network in cancer cells.[78] The CCKR signaling was strongly dysregulated by silencing of a lncRNA regulating the *TGM2* gene expression in another cancer cell line (MCF-7).[79] It has been disclosed that CCKR signaling is one of the enriched pathways promoting EMT in glioblastoma, with an increase of G-protein subunit gamma 2 (GNG2) by knockdown of GPR56.[41] We point out GNG2 (Supplementary Figure 2), belonging to PI3K-Akt signaling, that acquired an emerging role as tumor growth suppressor linked to survival in patients affected just by luminal A TNBC (such as MDA-MB-436).[47] We suppose that this effect could

depend on the GPR56-TG2 interaction.[80] Notably, GNG2 enhancing arrested the cell cycle and promoted apoptosis in BrCa cells inhibiting Akt and ERK functions through its interaction with MRAS.[47] Up-regulation of GNG2 by AA9 is consistent with apoptosis induction, previously described. However, in the CCKR signaling we underline overexpression of CXCL1, CXCL2, and MYC among the target genes, which must necessarily be kept under control to avoid the excessive production of proinflammatory chemokines.[81] A combined use of AA9 and novel drugs could be suggested.[82]

From a broader point of the view, we see that AA9 contrasts tumor cell behaviors. From a metabolic point of view, AA9 strongly inhibits glycolysis (Figure 3), with a wide number of down-regulated genes, leading to a decrease of the Warburg effect.[31] This pathway is interconnected with serine biosynthesis through PHGDH, which converts 3-phosphoglycerate to phosphohydroxypyruvate (PHP) reducing NAD^+, also connected with purine metabolism, another pathway impacted by AA9. Taken together, the intracellular AA9 impacts glycolysis, folic acid and purine biosynthesis, is crucial for cancer cells duplication. From the point of view of future potential therapy based on TG2-inhibitors, the combined use of molecules targeting PHGDH could be explored in an attempt to treat these aggressive forms of cancer.[82]

Based on the specific networks modulated by NCEG2, we can assume that the activity of extracellular TG2 protects and contains tumor expansion. Indeed, in MDA-MB-436 this kind of membrane-impermeable inhibitor induced the expression of transcripts coding proteins of replication and transcription machinery, such as DNA polymerase subunits, DNA topoisomerase, and RNAseH1, which remove hybrid DNA/RNA during mitochondrial genome replication and repair, and replication factor C, which have ATPase functions and are activated by antigen, promoting cell proliferation[83] (Supplementary Figure 3B). In this frame the only protein decreased was histone 3.5, a variant localized at transcription start sites generating unstable nucleosomes with a yet unknown role and only investigated in testicular cells associated with spermatogenesis.[84]

Interestingly, unique effects triggered by NCEG2 (partly shared with AA9) lead to modify the expression of ncRNAs (Figure 6). Nc-ANKRD36-1:8 and lnc-ANKRD36B-3:17 of still unknown functions were strongly up-regulated by NCEG2 in both cell lines, while both inhibitors induced overexpression of FP236383, ENSG00000274224 and FP671120 in MDA-MB-436 cells, and of the inflammation-related ncRNA AC083837.1 in MDA-MB-231 cells. Instead, LINC00887, the well-known biomarker of cell proliferation, was inversely modulated by the two inhibitors.

Analyzing early changes promoted by inhibitors that affect TG2 in specific cell compartments, we found specific and common pathways and gene networks with contrasting functions.

In conclusion, only AA9 is effective in both the employed aggressive cell lines (TNBC and p53-mutated) inducing apoptosis. Hence, intracellular TG2 promotes/supports the tumorigenicity of these BrCa cells, as recently reported by Gates *et al*.[39] However, anticancer efficacy tends to be eluded, suggesting that investigations should be addressed to test a combined use with compounds blocking specific genes to target characterizing networks, evidenced by this study and dependent on their cell-specific phenotype.

Surprisingly, the inhibition of TG2 outside the cell activates functions that favor cell proliferation and energy production, suggesting that TG2 mediates the containment of excessive tumor growth.

In light of the numerous pathologies in which TG2 is involved and of therapeutic applications, TG2 inhibitors are of considerable interest. The present work has clearly demonstrated that their localization must be taken into account.

In addition, this work disclosed the interconnection between TG2 activity and ncRNA expression associated with cancer behaviors, opening the way to a large field of new investigations.

It remains to be explored what intracellular functions are dependent exclusively on TG2 activity in the specific nuclear context and what are triggered by signaling cascades and assigned to the role of TG2 in other compartments.

Materials and Methods

Cell cultures

In this study we used TNBC MDA-MB-436 (RRID: CVCL_0623) and MDA-MB-231 (RRID: CVCL_0062) cells obtained from the American Type Culture Collection (Rockville, MD, USA). Cell cultures were assayed monthly for mycoplasma and other microorganism infections and quarterly for single-nucleotide polymorphism profile.

MDA-MB-436 are basal A, expressing considerable levels of cytokeratins and integrins, whereas MDA-MB-231 cells are more properly classified as basal B with up-regulated genes associated with invasive, aggressiveness, stemness features and proteins involved in the ECM remodeling.[85] These TNBC cell lines differ for some specific genomic mutations, MDA-MB-436 carried BRCA1 and RB1 mutations, while MDA-MB-231 shows BRAF, CD79A, CRTC3, CDKN2, KRAS, PDGFRA, and NF2. Both MDA-MB-436 and MDA-MB-231 cells are TP53-gene mutated.

Cells were harvested at 37 °C using DMEM High Glucose w/stable L-glutamine (EuroClone, Pero, Italy), containing 10% fetal bovine serum (Gibco Laboratories, New York, NY, USA) and penicillin/streptomycin solution (Merck Life Science), and

they were grown until achieving about 70% confluence. Before treatment, we replaced the medium and added the compounds AA9 and NCEG2 at 50 μM concentration. Since they must be resuspended in 0.1% DMSO (Merck KGa, Darmstadt, Germany), we used this vehicle as a control.

Transamidase activity assay

The transamidase activity of TG2 was analyzed in cytosolic lysate obtained from MDA-MB-231 and MDA-MB-436 cells exposed for 1 h to AA9 or NCEG2 at the concentration of 50 μM and then collected and tested for transamidase activity.

The extract preparation and the assays were carried out as reported and detailed by Gallo *et al.*[31] Briefly, we performed an *in situ* assay analyzing the transamidation of endogenous proteins after the addition of N-(5-aminopentyl)biotinamide trifluoroacetate salt (BAP) and exposure for 1 h to the inhibitors or only vehicle (0.1% DMSO). Cells were Ca^{2+}-permeabilized with A23187, collected, resuspended in buffer (50 mM TRIS, 150 mM NaCl, 1 mM EDTA, protease inhibitors and phenylmethylsulphonyl fluoride), and sonicated. Membranes were removed by centrifugation, then lysate proteins were quantified by the Bradford Protein Assay. The amount of biotin incorporated in cell substrates by transamidase reactions was detected by absorbing the homogenate proteins onto the wells of an ELISA plate and, after washing steps and blocking with BSA, reacting with HRP-conjugated streptavidin. The incorporated biotin was detected using 3,3′,5,5′-tetramethylbenzidine and hydrogen peroxide, and the reaction stopped with 2 M sulfuric acid. The absorbance was acquired at 450 nm with a 540 nm correction.

ELISA assay conditions

MDA-MB-231 and MDA-MB-436 cells untreated or treated with 50 μM AA9 or NCEG2 for 48 h was detached using scraper, washed twice with 1.5 mL of cold PBS, resuspended in 30 μL of cold buffer (50 mM TRIS, 150 mM NaCl, 1 mM EDTA, 1 μg/mL protease inhibitors (Halt™ Protease Inhibitor Cocktail Thermo Fisher Scientific), and 0.1 mM phenylmethylsulfonyl fluoride added at time of use).

After freezing of the cells, cellular lysates were recovered by centrifugation at 4000 g for 20 min, membranes were then precipitated by centrifugation, and the extracts quantified by BCA Protein Assay Kit (#23227, Thermo Scientific Pierce™, Segrate, MI, Italy), as well as the supernatants of the cell cultures. For the ELISA, 20 μg of total protein were assayed using ZediXclusive Tissue Transglutaminase EIA kit (Zedira GmbH, Darmstadt, Germany) of TG2, Human Matrix Metalloproteinase 1 (MMP1) kit and Human Collagen Type XIII kit (CliniSciences, Guidonia Montecelio, Rome, Italy). The assays were performed following the respective manufacturer's procedure.

GTP binding assay

GTP binding experiments were performed following a previously adapted protocol.[86] TG2 (60 μg) was incubated at 25 °C for 30 min with or without irreversible inhibitor (each at a concentration of 2 × K_I) with 15 mM $CaCl_2$ in 100 mM MOPS (pH = 6.91). The buffer was then exchanged by dialysis to 100 mM MOPS (pH = 7.0), 1 mM EGTA, and 5 mM $MgCl_2$ to remove calcium, using a 14-kDa molecular weight cut off membrane cuvette (Sigma-Aldrich). The fluorescent, nonhydrolyzable GTP analogue BODIPY GTP-γ-S (Invitrogen), whose fluorescence increases when bound to the protein, was then added at a final concentration of 0.5 μM. Fluorescence was then measured on a microplate reader after 10 min of incubation (Ex/Em: 490/520 nm).

Native PAGE assay

Native PAGE experiments were performed using a protocol adapted from those previously described[46]). TG2 (2.5 μM) was incubated at 25 °C for 30 min with or without irreversible inhibitor (each at a concentration of 2 × K_I) with 15 mM $CaCl_2$ in 100 mM MOPS (pH = 6.91). Three controls were performed: 1) uninhibited TG2 was analysed in the presence of calcium (100 mM MOPS + 15 mM $CaCl_2$ and in the absence of GTP; 2) uninhibited TG2 was analysed in the absence of both calcium and GTP; and 3) uninhibited TG2 was analysed in the presence of GTP (100 mM MOPS, 1 mM EGTA and 1 mM GTP but in the absence of calcium. A 20-μL aliquot (or 1.5 μg of TG2) of each solution was diluted with 20 μL of native Laemmli 2 × buffer (62.5 mM Tris-HCl (pH 6.8), 40% glycerol, 0.01% bromophenol blue), then 20 μL of each solution was loaded onto a 4–20% Mini-PROTEAN precast gel (Bio-Rad laboratoires, Ottawa, Ontario K1H 8 M5, Canada). The protein species were separated at 125 V for 90 min using running buffer without SDS (25 mM Tris, 192 mM glycine, pH 8.3) at 4 °C. The gel was stained using Coomassie brilliant blue R-250 solution, and de-stained with 10% acetic acid and 25% methanol in water.

Apoptosis assay

Apoptotic effects were analyzed using the Count & Viability kit (Prodottigianni, Milan, Italy) and MUSE cell analyzer. Cells were cultured in 2 mL well-plates and, after 24 h, treated with the inhibitors at 50 μM concentration, using the vehicle (0.1% DMSO) as controls. The cells were collected and resuspended in a medium containing 10% FBS. One hundred μL of cells (at least 5 × 10^5 cells/mL) were diluted 1:2 with

Annexin V & Dead Cell kit (Prodottigianni, Milan, Italy) to prepare the labeled cell samples, which were incubated for 20 min at room temperature, then analyzed by bioanalyzer.

RNA extraction, RNA-sequencing, and bioinformatic analysis

Transcriptome analysis was carried out on triplicate samples from both MDA-MB-436 and MDA-MB-231 cells treated with 50 μM AA9 or 50 μM NCEG2 and 0.1% DMSO, except for the duplicate control of MDA-MB-231 cells with 0.1% DMSO. After 24 h of exposure, the cells were detached with 0.05% Trypsin-EDTA (Gibco, Thermo Fisher Scientific, Milan, Italy), collected by centrifugation at 300 g for 10 min at 4 °C, and washed in PBS. Each sample ($\sim 3 \times 10^6$ cells) was resuspended in 1 mL of Trizol® Reagent (Merck KGa, Darmstadt, Germany), and 200 μL of chloroform (Merck KGa, Darmstadt, Germany) to allow the separation the solution into two phases by centrifugation at 3000 g for 15 min at 4 °C. RNA was recovered and precipitated from the aqueous phase by adding 500 μL of 2-*iso*-propanol (Thermo Fisher Scientific, Milan, Italy) for 20 min on ice, and collected at 3000 g for 20 min at 4 °C, resuspended in 1 mL of 75% ethanol. Finally, the pellet was recovered, dried and resuspended in nuclease free water (treated with diethyl pyrocarbonate, DEPC). Samples were stored at −80 °C until sequencing.

Samples were quantified and quality checked using a Qubit Bioanalyzer, and 1 μg of total RNA of each sample was used for sequencing by BMR Genomics (https://www.bmr-genomics.it, Padua, Italy). Library preparation was made with the Stranded mRNA Prep kit of Illumina, followed by the ribodepletion step using the QIAseq FastSelect-rRNA HMR kit (Qiagen, Milan, Italy). The mRNAs were captured via polyA tail and sequenced using the Illumina Novaseq 6000 platform, based on Next-Generation Sequencing technology obtaining 2 × 20 million reads/sample in 100PE format.

After the sequencing reaction, one fastq output file for each sample was produced, containing raw reads of transcripts. To undergo down-stream operations, raw reads required pre-processing steps carried out in a Linux environment with several bioinformatic tools; unprocessed data was reported (https://github.com/PietroAnc/VoliniaLab.git). First, we made a quality check of raw reads, a crucial operation to evaluate the appropriate removal of any sequencing reaction residuals. To check the quality of raw reads, we used the FastQC software [https://www.bioinformatics.babraham.ac.uk/projects/fastqc/], showing that the quality was optimal, so the trimming of 5′ or 3′ ends of reads was not necessary. The second step of bioinformatic processing was the alignment of reads to the GRCh38 reference genome using Bowtie2 software.[87] The latter produces a huge file (SAM) which was converted with Samtools software[88] into a BAM file, which is smaller and faster to analyze containing the same information as the former SAM. The next step was the counting of annotated transcripts in each sample. To run this analysis, we used FeatureCounts software[89] to obtain two files: a report containing statistical information and a text file embodying a count matrix containing transcript information, such as the name of the transcripts, chromosomal positions, strands, nucleotide lengths, and finally transcripts abundance.

To continue with gene expression analysis and to identify the dysregulated genes, it was necessary to modify the output files of FeatureCounts to make them compatible with the downstream pipeline. An "awk" script was employed in bash from the computer terminal to modify FeatureCounts files. Once ready, the count files were loaded onto RStudio [https://cran.rstudio.com]. The library chosen to perform differential expression analysis was DESeq2, ideal for analyzing data derived from RNA sequencing, especially if these follow a multinomial distribution approximated by the distribution of Poisson.[90] The software performed a differential expression analysis of the different samples, normalizing the reading values for each gene.

RStudio's DESeq2 package allowed us to identify early differentially expressed genes (DEGs) in the two experimental conditions, AA9 *vs* 0.1% DMSO (the control, vehicle) and NCEG2 *vs* 0.1% DMSO. Log2FC was used to measure the modulated specific transcripts, assuming as significant those with adjusted *p*-value < 0.05 (Benjamini-Hochberg correction, FDR $\leq$ 0.05).

CRGh38 was used as the reference genome to align the reads, while the annotation file was downloaded from https://www.ensembl.org/Homo_sapiens/Info/Index, containing more than 64,200 *meta*-features.

We used the list of differentially expressed genes generated from the DEGs analysis to carry out functional studies by two different approaches: the former is the GSEA to identify genes involved in the same pathways that have a significant and differential expression between the two experimental conditions (i.e. AA9 *vs* DMSO, or NCEG2 *vs* DMSO); the latter is the ORA to investigate whether, after the use of TG2 inhibitors, some pathways, belonging to a particular class of the Gene Ontology (GO) and sharing the same biological function, contain a larger enriched subset of genes than expected.

The pathways analysis was performed using the Panther Pathways database (https://www.pantherdb.org) in the WebGestalt webtool [https://www.webgestalt.org]. Finally, with the output data of the functional analysis we created interconnections using NetworkAnalyst 3.0,

representing the modulated pathways by the treatment with the two investigated molecules.[91]

Primers and conditions of RT-qPCR

We used 1 μg of total RNA to carry out reverse transcription by TaqMan™ Reverse Transcription Reagents kit (Thermo FisherScientific, Monza, MI, Italy). Fifty ng of cDNA were amplified with the following primers, of which we intended to validate the expression, at the final 150 nM, and designed by means of Primer-BLAST software (site https://www.ncbi.nlm.nih.gov/tools/primer-blast, accessed on 7 October 2023): RHOBF, 5′-GAGAACATCCCC GAGAAGTG-3′ and ROBR, 5′-CTTCCTTGGTCT TGGCAGA-3′; MMP1F, 5′-GCTGCTTAC GAATTTGCCGA-3′ and MMP1R, 5′-GGGGTATC CGTGTAGCACAT-3′; AKT2F 5′-ACAAGGAAAGG GAACCAGCG-3′ and AKT2R 5′-GGTACGCTGT CACCTAGCTC-3′.

Amplification reactions were carried out in the presence of 20 μL of PowerUp™ SYBR® Green Master Mix (Thermo FisherScientific, Monza, MI, Italy) employing the thermal cycler CFX96 Touch™ Real-Time PCR Detection System (Bio-rad Laboratories Srl, Segrate, Milan, Italy). Quantification of gene expression was achieved applying the FC formula $2^{-\Delta\Delta CT}$ using actin as housekeeping.

Immunochemical analysis

The cells treated with TG2 inhibitors for 48 h were lysed with RIPA buffer and quantified by BCA Protein Assay Kit (#23227, Thermo Scientific Pierce™, Segrate (MI), Italy). Total cell lysates from MDA-MB-436 cells under different experimental conditions were separated on 12.5% denaturing polyacrylamide gels and blotted to nitrocellulose membranes (GE Healthcare Life Science, Milan, Italy). All antibodies were obtained from Merck KGa (Darmstadt, Germany), and hybridization was performed using anti-GNG2 (cat. HPA003534) and anti-β-Tubulin (cat. T4026), following the manufacturer's instructions.

The immune complexes were detected by chemiluminescence using the WESTAR NOVA 2.0 ECL system (Cyanagen, Bologna, Italy), acquired with an ImageQuantTM LAS 4000 biomolecular imager (GE Healthcare Life Science) and densitometry used to quantify the bands was performed using Image Quant TL software (GE Healthcare Life Science), as previously reported.[92]

CRediT authorship contribution statement

Pietro Ancona: Software, Methodology, Investigation, Formal analysis. **Alessandro Trentini:** Methodology, Investigation, Formal analysis. **Anna Terrazzan:** Software, Methodology, Investigation, Formal analysis. **Silvia Grassilli:** Validation, Resources, Methodology. **Pauline Navals:** Investigation, Methodology. **Eric W.J. Gates:** Writing – review & editing, Methodology. **Valentina Rosta:** Methodology. **Carlo Cervellati:** Writing – review & editing. **Carlo M. Bergamini:** Writing – original draft, Supervision, Investigation, Data curation. **Angela Pignatelli:** Resources, Funding acquisition. **Jeffrey W. Keillor:** Writing – review & editing, Investigation, Conceptualization. **Cristian Taccioli:** Writing – review & editing, Resources, Funding acquisition. **Nicoletta Bianchi:** Writing – original draft, Supervision, Project administration, Investigation, Funding acquisition, Conceptualization.

DECLARATION OF COMPETING INTEREST

The authors declare that they have no known competing financial interests or personal relationships that could have appeared to influence the work reported in this paper.

Acknowledgments

This research was supported by the following grants: Nicoletta Bianchi by Fondo per l'Incentivazione alla Ricerca FIR2021 (FIR2191318) and Fondo Interdisciplinare per la Ricerca Dipartimentale FIRD2022 (2022-FAR.L-FIRD_medtras_Brugnoli); Silvia Grassilli by FIRD2023: (2023-FAR.L-FIRD_medtras_Grassilli); Angela Pignatelli by PRIN 2009 (2019-PRA.A-PA_001_Pignatelli); Cristian Taccioli by BIRD213010/21. Finally, we would like to thank the Laboratorio per le Tecnologie delle Terapie Avanzate of the University of Ferrara and Co.Pe.Go. (Soc.Coop.O.P.) for the liberal voluntary contribution to the present research and Deborah Ancona for the graphical abstract.

Appendix A. Supplementary data

Supplementary data to this article can be found online at https://doi.org/10.1016/j.jmb.2024.168569.

Received 28 December 2023;
Accepted 5 April 2024;
Available online 10 April 2024

Keywords:
transglutaminase type 2;
AA9;
NGEG2;
MDA-MB-436;
MDA-MB-231

Abbreviations used:
ACOX2, Acyl-CoA oxidase 2; ARRDC4, arrestin domain

containing 4; ATPF, ATP synthase F complex; BAP, N-(5-aminopentyl)biotinamide; BEST1, Bestrophin-1; BMP, bone morphogenetic protein; BrCa, breast cancer; CADM2, cell adhesion molecule 2; CCKR, gastrin and cholecystokinin receptors; CDKN1A, cyclin-dependent kinase inhibitor 1A; CTNNA2, αN-catenin; DEGs, differentially expressed genes; ECM, extracellular matrix; FC, Fold Change; FDR, false discovery rate; FTH1, ferritin heavy chain 1; GO, Gene Ontology; GNG2, G protein subunit gamma 2; GDF15, growth differentiation factor 15; GSEA, Gene Set Enrichment Analysis; HAS2, Hyaluronan Synthase 2; HMOX1, heme oxygenase 1; KRTAP2-3, keratin-associated protein 2–3; LAMB2P1, laminin subunit beta 2 pseudogene 1; lncRNA, long non-coding RNA; MMPs, matrix metalloproteinases; NFKBIA, NF-κB inhibitor α; ncRNA, non-coding RNA; ORA, Over Representation Analysis; PCA, principal component analysis; PHGDH, phosphoglycerate dehydrogenase; PHP, phosphohydroxypyruvate; ROS, reactive oxygen species; SCARA3, Scavenger receptor class A, member 3; SGPP2, sphingosine-1-phosphate phosphatase; RHBDL1, Rhomboid Like 1; RT-qPCR, reverse-transcription and quantitative polymerase chain reaction; TG2, transglutaminase 2; TNBC, triple-negative BrCa cells; TNFAIP3, TNFα-induced protein 3; TNFRSF9, tumor necrosis factor receptor; *vs*, *versus*; XDH, Xanthine dehydrogenase

References

1. Hettasch, J.M., Bandarenko, N., Burchette, J.L., Lai, T.S., Marks, J.R., Haroon, Z.A., et al., (1996). Tissue transglutaminase expression in human breast cancer. *Lab. Invest.* **75**, 637–645.
2. Assi, J., Srivastava, G., Matta, A., Chang, M.C., Walfish, P. G., Ralhan, R., (2013). Transglutaminase 2 overexpression in tumor stroma identifies invasive ductal carcinomas of breast at high risk of recurrence. *PLoS One* **8**, e74437.
3. Ai, L., Kim, W.J., Demircan, B., Dyer, L.M., Bray, K.J., Skehan, R.R., et al., (2008). The transglutaminase 2 gene (TGM2), a potential molecular marker for chemotherapeutic drug sensitivity, is epigenetically silenced in breast cancer. *Carcinogenesis* **29**, 510–518.
4. Liu, T., Tee, A.E., Porro, A., Smith, S.A., Dwarte, T., Liu, P. Y., et al., (2007). Activation of tissue transglutaminase transcription by histone deacetylase inhibition as a therapeutic approach for Myc oncogenesis. *PNAS* **104**, 18682–18687.
5. Cao, J., Huang, W., (2016). Compensatory increase of transglutaminase 2 is responsible for resistance to mTOR inhibitor treatment. *PLoS One* **11**, e0149388.
6. Shinde, A., Kulkoyluoglu Cotul, E., Chen, H., Smith, A., Libring, S., Solorio, L., et al., (2022). Transglutaminase-2 mediates acquisition of neratinib resistance in metastatic breast cancer. *Mol. Biomed.* **3**, 19–30.
7. Cheng, K., Wang, X.H., Hua, Y.T., Zhang, Y.Z., Han, Y., Yang, Z.L., (2020). The tissue transglutaminase: a potential target regulating MDR in breast cancer. *Eur. Rev. Med. Pharmacol. Sci.* **24**, 6175–6184.
8. Fisher, M.L., Adhikary, G., Xu, W., Kerr, C., Keillor, J.W., Eckert, R.L., (2015). Type II transglutaminase stimulates epidermal cancer stem cell epithelial-mesenchymal transition. *Oncotarget* **6**, 20525–20539.
9. Karicheva, O., Rodriguez-Vargas, J.M., Wadier, N., Martin-Hernandez, K., Vauchelles, R., Magroun, N., et al., (2016). PARP3 controls TGFβ and ROS driven epithelial-to-mesenchymal transition and stemness by stimulating a TG2-Snail-E-cadherin axis. *Oncotarget* **7**, 64109–64123.
10. Eckert, R.L., Fisher, M.L., Grun, D., Adhikary, G., Xu, W., Kerr, C., (2015). Transglutaminase is a tumor cell and cancer stem cell survival factor. *Mol. Carcinog.* **54**, 947–958.
11. Mehta, K., Fok, J., Miller, F.R., Koul, D., Sahin, A.A., (2004). Prognostic significance of tissue transglutaminase in drug resistant and metastatic breast cancer. *Clin. Cancer Res.* **10**, 8068–8076.
12. Li, B., Antonyak, M.A., Druso, J.E., Cheng, L., Nikitin, A.Y., Cerione, R.A., (2010). EGF potentiated oncogenesis requires a tissue transglutaminase-dependent signaling pathway leading to Src activation. *PNAS* **107**, 1408–1413.
13. Agnihotri, N., Kumar, S., Mehta, K., (2013). Tissue transglutaminase as a central mediator in inflammation-induced progression of breast cancer. *Breast Cancer Res.* **15**, 202–211.
14. Park, K.S., Kim, D.S., Jeong, K.C., Kim, S.Y., (2009). Increase in transglutaminase 2 expression is associated with NF-kappaB activation in breast cancer tissues. *Front. Bioscience (landmark Ed.)* **14**, 1945–1951.
15. Brown, K.D., (2013). Transglutaminase 2 and NF-κB: an odd couple that shapes breast cancer phenotype. *Breast Cancer Res. Treat.* **137**, 329–336.
16. Oh, K., Lee, O.Y., Park, Y., Seo, M.W., (2016). IL-1β induces IL-6 production and increases invasiveness and estrogen-independent growth in a TG2-dependent manner in human breast cancer cells. *BMC Cancer* **16**, 724–735.
17. Sima, L.E., Matei, D., Condello, S., (2022). The outside-in journey of tissue transglutaminase in cancer. *Cells* **11**, 1779–1803.
18. Kim, D.S., Han, B.G., Park, K.S., Lee, B.I., Kim, S.Y., Bae, C.D., (2010). I-kappaBalpha depletion by transglutaminase 2 and mu-calpain occurs in parallel with the ubiquitin-proteasome pathway. *Biochem. Biophys. Res. Commun.* **399**, 300–306.
19. Yakubov, B., Chelladurai, B., Schmitt, J., Emerson, R., Turchi, J.J., Matei, D., (2013). Extracellular tissue transglutaminase activates noncanonical NF-κB signaling and promotes metastasis in ovarian cancer. *Neoplasia* **15**, 609–619.
20. Wang, Z., Griffin, M., (2013). The role of TG2 in regulating S100A4-mediated mammary tumour cell migration. *PLoS One* **8**, e57017.
21. Libring, S., Shinde, A., Chanda, M.K., Nuru, M., George, H., Saleh, A.M., et al., (2020). The dynamic relationship of breast cancer cells and fibroblasts in fibronectin accumulation at primary and metastatic tumor sites. *Cancers* **12**, 1270–1290.
22. Shinde, A., Paez, J.S., Libring, S., Hopkins, K., Solorio, L., Wendt, M.K., (2020). Transglutaminase-2 facilitates extracellular vesicle-mediated establishment of the metastatic niche. *Oncogenesis* **9**, 16–28.
23. Eckert, R.L., Kaartinen, M.T., Nurminskaya, M., Belkin, A. M., Colak, G., Johnson, G.V., et al., (2014). Transglutaminase regulation of cell function. *Physiol. Rev.* **94**, 383–417.
24. Bianchi, N., Brugnoli, F., Grassilli, S., Bourgeois, K., Keillor, J.W., Bergamini, C.M., et al., (2021). The motility and mesenchymal features of breast cancer cells correlate with

the levels and intracellular localization of transglutaminase type 2. *Cells* **10**, 3059–3078.
25. Canella, R., Brugnoli, F., Gallo, M., Keillor, J.W., Terrazzan, A., Ferrari, E., et al., (2022). A multidisciplinary approach establishes a link between transglutaminase 2 and the Kv10.1 voltage-dependent K+ channel in breast cancer. *Cancers* **15**, 178–197.
26. Kumar, A., Xu, J., Sung, B., Kumar, S., Yu, D., Aggarwal, B.B., et al., (2012). Evidence that GTP-binding domain but not catalytic domain of transglutaminase 2 is essential for epithelial-to-mesenchymal transition in mammary epithelial cells. *Breast Cancer Res.* **14**, R4.
27. Lin, H.Y., Kuei, C.H., Lee, H.H., Lin, C.H., Zheng, J.Q., Chiu, H.W., et al., (2020). The Gαh/phospholipase C-δ1 interaction promotes autophagosome degradation by activating the Akt/mTORC1 pathway in metastatic triple-negative breast cancer. *Aging* **12**, 13023–13037.
28. Martins, F.C., Teixeira, F., Reis, I., Geraldes, N., Cabrita, A.M., Dias, M.F., (2009). Increased transglutaminase 2 and GLUT-1 expression in breast tumors not susceptible to chemoprevention with antioxidants. *Tumori* **95**, 227–232.
29. Kumar, S., Donti, T.R., Agnihotri, N., Mehta, K., (2014). Transglutaminase 2 reprogramming of glucose metabolism in mammary epithelial cells via activation of inflammatory signaling pathways. *Int. J. Cancer* **134**, 2798–2807.
30. Xu, D., Xu, N., Sun, L., Yang, Z., He, M., Li, Y., (2022). TG2 as a novel breast cancer prognostic marker promotes cell proliferation and glycolysis by activating the MEK/ERK/LDH pathway. *BMC Cancer* **22**, 1267–1278.
31. Gallo, M., Ferrari, E., Terrazzan, A., Brugnoli, F., Spisni, A., Taccioli, C., et al., (2023). Metabolic characterisation of transglutaminase 2 inhibitor effects in breast cancer cell lines. *FEBS J.* **290**, 5411–5433.
32. Dalby, K.N., Tekedereli, I., Lopez-Berestein, G., Ozpolat, B., (2010). Targeting the prodeath and prosurvival functions of autophagy as novel therapeutic strategies in cancer. *Autophagy* **6**, 322–329.
33. Kim, D.S., Park, S.S., Nam, B.H., Kim, I.H., Kim, S.Y., (2006). Reversal of drug resistance in breast cancer cells by transglutaminase 2 inhibition and nuclear factor-kappaB inactivation. *Cancer Res.* **66**, 10936–10943.
34. Datta, S., Antonyak, M.A., Cerione, R.A., (2006). Importance of Ca(2+)-dependent transamidation activity in the protection afforded by tissue transglutaminase against doxorubicin-induced apoptosis. *Biochemistry* **45**, 13163–13174.
35. He, W., Sun, Z., Liu, Z., (2015). Silencing of TGM2 reverses epithelial to mesenchymal transition and modulates the chemosensitivity of breast cancer to docetaxel. *Exp. Ther. Med.* **10**, 1413–1418.
36. Zhuang, J., Liang, S., Chen, L., Yang, F., Huo, Q., Wu, M., Zhang, Y., Xie, N., (2021). Utilizing a high-throughput microdevice to study breast tumor cells clustering and metastasis. *Anal. Chim. Acta* **1151**, 338222–338230.
37. Kim, D.S., Park, K.S., Kim, S.Y., (2009). Silencing of TGase 2 sensitizes breast cancer cells to apoptosis by regulation of survival factors. *Front. Biosci. (landmark Ed.)* **14**, 2514–2521.
38. Choi, J., Lee, H.J., Yoon, S., Ryu, H.M., Lee, E., Jo, et al., (2020). Blockade of CCL2 expression overcomes intrinsic PD-1/PD-L1 inhibitor-resistance in transglutaminase 2-induced PD-L1 positive triple negative breast cancer. *Am. J. Cancer Res.* **10**, 2878–2894.
39. Gates, E.W.J., Calvert, N.D., Cundy, N.J., Brugnoli, F., Navals, P., Kirby, A., et al., (2023). Cell-impermeable inhibitors confirm that intracellular human transglutaminase 2 is responsible for the transglutaminase-associated cancer phenotype. *Int. J. Mol. Sci.* **24**, 12546–12564.
40. Mangala, L.S., Arun, B., Sahin, A.A., Mehta, K., (2005). Tissue transglutaminase-induced alterations in extracellular matrix inhibit tumor invasion. *Mol. Cancer* **4**, 33–41.
41. Ganesh, R.A., Sonpatki, P., Naik, D., John, A.E., Sathe, G., Lakshmikantha, A., et al., (2022). Multi-omics analysis of glioblastoma and glioblastoma cell line: molecular insights into the functional role of GPR56 and TG2 in mesenchymal transition. *Front. Oncol.* **12**, 841890–841910.
42. L'Heureux, D.Z., Rothman, V.L., Tuszynski, G.P., (2010). The interaction of angiocidin with tissue transglutaminase. *Exp. Mol. Path.* **88**, 15–25.
43. Enciso-Benavides, J., Alfaro, L., Castañeda-Altamirano, C., Rojas, N., González-Cabeza, J., Enciso, N., et al., (2021). Biological characteristics of a sub-population of cancer stem cells from two triple-negative breast tumour cell lines. *Heliyon* **7**, e07273.
44. Thompson, E.W., Paik, S., Brünner, N., Sommers, C.L., Zugmaier, G., Clarke, R., et al., (1992). Association of increased basement membrane invasiveness with absence of estrogen receptor and expression of vimentin in human breast cancer cell lines. *J. Cell. Physiol.* **150**, 534–544.
45. Caudroy, S., Polette, M., Nawrocki-Raby, B., Cao, J., Toole, B.P., Zucker, S., Birembaut, P., (2002). EMMPRIN-mediated MMP regulation in tumor and endothelial cells. *Clin. Exp. Metastasis* **19**, 697–702.
46. Begg, G.E., Carrington, L., Stokes, P.H., Matthews, J.M., Wouters, M.A., Husain, A., et al., (2006). Mechanism of allosteric regulation of transglutaminase 2 by GTP. *PNAS* **103**, 19683–19688.
47. Zhao, A., Li, D., Mao, X., Yang, M., Deng, W., Hu, W., et al., (2022). GNG2 acts as a tumor suppressor in breast cancer through stimulating MRAS signaling. *Cell Death Dis.* **13**, 260.
48. Wu, H., Huang, X., Chen, S., Li, S., Feng, J., Zouxu, X., et al., (2020). Comprehensive analysis of the NME gene family functions in breast cancer. *Transl. Cancer Res.* **9**, 6369–6382.
49. Ali, A., Shafarin, J., Abu Jabal, R., Aljabi, N., Hamad, M., Sualeh Muhammad, J., et al., (2021). Ferritin heavy chain (FTH1) exerts significant antigrowth effects in breast cancer cells by inhibiting the expression of c-MYC. *FEBS Open Bio* **11**, 3101–3114.
50. Laurenzi, V., Melino, G., (2002). Gene disruption of tissue transglutaminase. *Mol. Cell Biol.* **21**, 148–155.
51. Odii, B.O., Coussons, P., (2014). Biological functionalities of transglutaminase 2 and the possibility of its compensation by other members of the transglutaminase family. *ScientificWorldJournal* **2014**, 714561–714574.
52. Schuppan, D., Mäki, M., Lundin, K.E.A., Isola, J., Friesing-Sosnik, T., Taavela, J., et al., (2021). CEC-3 Trial Group. A randomized trial of a transglutaminase 2 inhibitor for celiac disease. *N. Engl. J. Med.* **385**, 35–45.
53. Isola, J., Mäki, M., Hils, M., Pasternack, R., Viiri, K., Dotsenko, V., et al., (2023). The oral transglutaminase 2 inhibitor ZED1227 accumulates in the villous enterocytes in celiac disease patients during gluten challenge and drug treatment. *Int. J. Mol. Sci.* **24**, 10815–10826.

54. Hu, Z., Li, X., Yuan, R., Ring, B.Z., Su, L., (2010). Three common TP53 polymorphisms in susceptibility to breast cancer, evidence from meta-analysis. *Breast Cancer Res. Treat.* **120**, 705–714.
55. Wasielewski, M., Elstrodt, F., Klijn, J.G., Berns, E.M., Schutte, M., (2006). Thirteen new p53 gene mutants identified among 41 human breast cancer cell lines. *Breast Cancer Res. Treat.* **99**, 97–101.
56. Liu, X., Zhou, Y., Qin, C., Zhu, X., (2022). TNFRSF9 suppressed the progression of breast cancer via the p38MAPK/PAX6 signaling pathway. *J. Oncol.* **2022**, 8549781–8549797.
57. Parvani, J.G., Davuluri, G., Wendt, M.K., Espinosa, C., Tian, M., Danielpour, D., et al., (2015). Deptor enhances triple-negative breast cancer metastasis and chemoresistance through coupling to survivin expression. *Neoplasia* **17**, 317–328.
58. Maemura, M., Akiyama, S.K., Woods Jr., V.L., Dickson, R. B., (1995). Expression and ligand binding of alpha 2 beta 1 integrin on breast carcinoma cells. *Clin. Exp. Metastasis* **13**, 223–235.
59. Subbaram, S., Dipersio, C.M., (2011). Integrin alpha3beta1 as a breast cancer target. *Expert Opin. Ther. Targets* **15**, 1197–1210.
60. Zhang, D.X., Dang, X.T.T., Vu, L.T., Lim, C.M.H., Yeo, E.Y. M., Lam, B.W.S., et al., (2022). Alphavbeta1 integrin is enriched in extracellular vesicles of metastatic breast cancer cells: A mechanism mediated by galectin-359. *J. Extracell. Vesicles* **11**, e12234.
61. Gwili, N., Jones, S.J., Amri, W.A., Carr, I.M., Harris, S., Hogan, B.V., et al., (2021). Transcriptome profiles of stem-like cells from primary breast cancers allow identification of ITGA7 as a predictive marker of chemotherapy response. *Br. J. Cancer* **125**, 983–993.
62. Pin, A.L., Huot, J., (2010). Beta5 integrin orchestrates epithelial mesenchymal transition in breast cancer: comment on: Bianchi A, et al. *Cell Cycle* **9**, 1647–1659.
63. Zhao, D., Qiao, J., He, H., Song, J., Zhao, S., Yu, J., (2020). TFPI2 suppresses breast cancer progression through inhibiting TWIST-integrinalpha5 pathway. *Mol. Med.* **26**, 27–37.
64. Hu, T., Zhou, R., Zhao, Y., Wu, G., (2016). Integrinalpha6/Akt/Erk signaling is essential for human breast cancer resistance to radiotherapy. *Sci. Rep.* **6**, 33376–33386.
65. Zemskov, E.A., Janiak, A., Hang, J., Waghray, A., Belkin, A.M., (2006). The role of tissue transglutaminase in cell-matrix interactions. *Front. Biosci.* **11**, 1057–1076.
66. Condello, S., Prasad, M., Atwani, R., Matei, D., (2022). Tissue transglutaminase activates integrin-linked kinase and beta-catenin in ovarian cancer. *J. Biol. Chem.* **298**, 102242–102259.
67. Benhaj, K., Akcali, K.C., Ozturk, M., (2006). Redundant expression of canonical Wnt ligands in human breast cancer cell lines. *Oncol. Rep.* **15**, 701–707.
68. Xiang, Y., Lin, G., Zhang, Q., Tan, Y., Lu, G., (2008). Knocking down Wnt9a mRNA levels increases cellular proliferation. *Mol. Biol. Rep.* **35**, 73–79.
69. Goto, H., Kosako, H., Tanabe, K., Yanagida, M., Sakurai, M., Amano, M., et al., (1998). Phosphorylation of vimentin by Rho-associated kinase at a unique amino-terminal site that is specifically phosphorylated during cytokinesis. *J. Biol. Chem.* **273**, 11728–11736.
70. Privat, M., Cavard, A., Zekri, Y., Ponelle-Chachuat, F., Molnar, I., Sonnier, N., et al., (2020). A high expression ratio of RhoA/RhoB is associated with the migratory and invasive properties of basal-like breast tumors. *Int. J. Med. Sci.* **17**, 2799–2808.
71. Belkin, A.M., Akimov, S.S., Zaritskaya, L.S., Ratnikov, B.I., Deryugina, E.I., Strongin, A.Y., (2001). Matrix-dependent proteolysis of surface transglutaminase by membrane-type metalloproteinase regulates cancer cell adhesion and locomotion. *J. Biol. Chem.* **276**, 18415–18422.
72. Cheng, T., Chen, P., Chen, J., Deng, Y., Huang, C., (2022). Landscape analysis of matrix metalloproteinases unveils key prognostic markers for patients with breast cancer. *Front. Genet.* **12**, 809600–809615.
73. Llinàs-Arias, P., Ensenyat-Mendez, M., Íñiguez-Muñoz, S., Orozco, J.I.J., Valdez, B., Salomon, M.P., et al., (2023). Chromatin insulation orchestrates matrix metalloproteinase gene cluster expression reprogramming in aggressive breast cancer tumors. *Mol. Cancer* **22**, 190–224.
74. Kamalabadi Farahani, M., Atashi, A., Bitaraf, F.S., (2023). Upregulation of matrix metalloproteinases in the metastatic cascade of breast cancer to the brain. *Asian Pac. J. Cancer Prev.* **24**, 2997–3001.
75. Parveen, S., Khamari, A., Raju, J., Coppolino, M.G., Datta, S., (2022). Syntaxin 7 contributes to breast cancer cell invasion by promoting invadopodia formation. *J. Cell Sci.* **135**, jcs259576.
76. Rizki, A., Weaver, V.M., Lee, S.Y., Rozenberg, G.I., Chin, K., Myers, C.A., et al., (2008). A human breast cell model of preinvasive to invasive transition. *Cancer Res.* **68**, 1378–1387.
77. Jones, R.A., Kotsakis, P., Johnson, T.S., Chau, D.Y., Ali, S., Melino, G., Griffin, M., (2006). Matrix changes induced by transglutaminase 2 lead to inhibition of angiogenesis and tumor growth. *Cell Death Differ.* **13**, 1442–1453.
78. Tripathi, S., Flobak, Å., Chawla, K., Baudot, A., Bruland, T., Thommesen, L., et al., (2015). The gastrin and cholecystokinin receptors mediated signaling network: a scaffold for data analysis and new hypotheses on regulatory mechanisms. *BMC Sys. Biol.* **9**, 40–55.
79. Bergamini, C.M., Vischioni, C., Aguiari, G., Grandi, C., Terrazzan, A., Volinia, S., et al., (2021). Inhibition of the lncRNA coded within transglutaminase 2 gene impacts several relevant networks in MCF-7 breast cancer cells. *Non-Coding RNA* **7**, 49–68.
80. Salzman, G.S., Zhang, S., Fernandez, C.G., Araç, D., Koide, S., (2020). Specific and direct modulation of the interaction between adhesion GPCR GPR56/ADGRG1 and tissue transglutaminase 2 using synthetic ligands. *Sci. Rep.* **10**, 16912–16921.
81. Lin, F.T., Liu, K., Garan, L.A.W., Folly-Kossi, H., Song, Y., Lin, S.J., et al., (2023). A small-molecule inhibitor of TopBP1 exerts anti-MYC activity and synergy with PARP inhibitors. *PNAS* **120**, e2307793120
82. McNamee, M.J., Michod, D., Niklison-Chirou, M.V., (2021). Can small molecular inhibitors that stop de novo serine synthesis be used in cancer treatment? *Cell Death Discov.* **7**, 87.
83. Cullmann, G., Fien, K., Kobayashi, R., Stillman, B., (1995). Characterization of the five replication factor C genes of Saccharomyces cerevisiae. *Mol. Cell Biol.* **15**, 4661–4671.
84. Urahama, T., Harada, A., Maehara, K., Horikoshi, N., Sato, K., Sato, Y., et al., (2016). Histone H3.5 forms an unstable nucleosome and accumulates around transcription start sites in human testis. *Epigenet. Chromat.* **9**, 2–18.

85. Dai, X., Cheng, H., Bai, Z., Li, J., (2017). Breast cancer cell line classification and its relevance with breast tumor subtyping. *J. Cancer* **8**, 3131–3141.
86. Akbar, A., McNeil, N.M.R., Albert, M.R., Ta, V., Adhikary, G., Bourgeois, K., et al., (2017). Structure-activity relationships of potent, targeted covalent inhibitors that abolish both the transamidation and GTP binding activities of human tissue transglutaminase. *J. Med. Chem.* **60**, 7910–7927.
87. Li, H., Durbin, R., (2009). Fast and accurate short read alignment with Burrows-Wheeler transform. *Bioinformatics* **25**, 1754–1760.
88. Li, H., Handsaker, B., Wysoker, A., Fennell, T., Ruan, J., Homer, N., 1000 Genome Project Data Processing Subgroup, et al., (2009). The sequence alignment/map format and SAMtools. *Bioinformatics (Oxford, England)* **25**, 2078–2079.
89. Liao, Y., Smyth, G.K., Shi, W., (2014). featureCounts: an efficient general-purpose program for assigning sequence reads to genomic features. *Bioinformatics* **30**, 923–930.
90. Love, M.I., Huber, W., Anders, S., (2014). Moderated estimation of fold change and dispersion for RNA-seq data with DESeq2. *Genome Biol.* **15**, 550–571.
91. Zhou, G., Soufan, O., Ewald, J., Hancock, R.E.W., Basu, N., Xia, J., (2019). NetworkAnalyst 3.0: a visual analytics platform for comprehensive gene expression profiling and meta-analysis. *Nucleic Acids Res.* **47**, 234–241.
92. Volinia, S., Bertagnolo, V., Grassilli, S., Brugnoli, F., Manfrini, M., Galasso, M., et al., (2018). Levels of miR-126 and miR-218 are elevated in ductal carcinoma in situ (DCIS) and inhibit malignant potential of DCIS derived cells. *Oncotarget* **9**, 23543–23553.